

Food-Based Edible Electronics

by

Haokai Yang

A Dissertation Presented in Partial Fulfillment
of the Requirements for the Degree
Doctor of Philosophy

Approved April 2021 by the
Graduate Supervisory Committee:

Hanqing Jiang, Co-Chair
Hongbin Yu, Co-Chair
Yu Yao
Qiong Nian
Houlong Zhuang

ARIZONA STATE UNIVERSITY

May 2021

ABSTRACT

A new class of electronic materials from food and foodstuff was developed to form a “toolkit” for edible electronics along with inorganic materials. Electrical components like resistors, capacitors and inductors were fabricated with such materials and tested. Applicable devices such as filters, microphones and pH sensors were built with edible materials. Among the applications, a wireless edible pH sensor was optimized in terms of form factor, fabrication process and cost.

This dissertation discusses the material sciences of food industry, design and fabrication of electronics and biomedical engineering by demonstrating edible electronic materials, components and devices such as filters, microphones and pH sensors. pH sensors are optimized for two different generations of design and fabrication.

DEDICATION

I dedicate my dissertation to my family, my parents Yueshuang Li and Guoyou Yang who have supported me emotionally and financially over decades, my wife Taylor Yang who has brought joys and strengths in my life.

ACKNOWLEDGMENTS

I would like to thank my supervisors Prof. Hanqing Jiang and Prof. Hongbin Yu, who have both always supported me for about six years. They teach me the methodology of how to tackle research. There're times when my experiments not going successful, and Prof. Jiang is patient to me and guides me through pivots and validations of potential solutions. Prof. Yu has taught me fundamentals to solve the problems whenever I needed. Having both amazing mentors makes me who I am as an engineer.

I'm grateful for the helps from my committee members, Prof. Yu Yao, Prof. Qiong Nian and Prof. Houlong Zhuang.

I'd love to thank my colleagues at Arizona State University, Dr. Xu Wang, Dr. Wenwen Xu, Dr. Zeming Song, Dr. Cheng Lv, Dr. Wei Zeng, Todd Houghton, Zhizhou He, Zirui Zhai.

TABLE OF CONTENTS

	Page
LIST OF TABLES	v
LIST OF FIGURES	vi
1 INTRODUCTION	1
2 FOOD BASED EDIBLE AND NUTRITIVE ELECTRONICS.....	3
2.1. Background and Motivations	3
2.2. Experimental Section.....	5
2.2.1. Preparation of the Materials	5
2.2.2. Preparation of Shadow Mask	5
2.2.3. Preparation of Electrical Components	5
2.2.4. Preparation of Samples for Mechanical Test.....	7
2.2.5. Characterization of Materials, Components, And Devices	8
2.2.6. Mechanical Characterization of Food Materials as Structural Functions	9
2.2.7. Characterization of the Piezoelectric Coupling Coefficient.....	9
2.3. Result and Discussion	11
3 EDIBLE WIRELESS PH SENSORS: VERSION 1	25
3.1. Background and Motivation	25
3.2. Mechanism of the Edible pH Sensor	26
3.3. Experimental Section.....	27
3.3.1. Fabrication of the pH Sensor	27
3.3.2. Characterization of the pH Sensor	28
3.4. Result and Discussion	29
4 EDIBLE WIRELESS PH SENSORS: VERSION 2	32
4.1. Introduction	32
4.2. Design of Electrodes.....	34
4.3. Design of Inductor.....	36
4.4. Fabrication of the pH sensor	52
4.5. Characterization of the pH sensor	53
4.6. Result and Discussion	59
5 SUMMARY AND FUTURE WORK.....	63
5.1. Summary	63
5.2. Future Work	64
REFERENCES	66

LIST OF TABLES

Table	Page
Table 2.1 Comprehensive List of Conductivity of Commonly Accessible Food Materials	13
Table 2.2 Conductivity of Processed Food Materials	15
Table 2.3 D33 of Different Piezoelectric Materials	17
Table 2.4 A Toolkit Using Food-Based Materials to Build Necessary Electrical Components.....	18
Table 4.1 Conductivity of Processed Food Materials	35
Table 4.2 Inductances with Different Length, Width and Metal-Trace Width	40
Table 4.3 Inductances with Different Angles	41
Table 4.4 Examples of Designs of Reading Antennas	57
Table 4.5 Parasitic Capacitance of Rolled Inductor.	43

LIST OF FIGURES

Figure	Page
Figure 2.1 “Sandwich” Structure for Electrical Conductivity Measurement	8
Figure 2.2 Sample Holder for Electrical Conductivity Measurement for Liquid Materials.	8
Figure 2.3 Schematic of the Characterization Of D33.	10
Figure 2.4 (A) Equipment Set Up for Characterization of D31. (B) Sample and Electrode Design.	10
Figure 2.5 Selections and Characterizations of Food-Based Materials Regarding Their Electronical Properties. (A) A Typical Food Pyramid With Conductivities and Dielectric Constants of Some Representative Food Materials According to Recognized Food Groups. The Shaded Elements Represent Food Materials that Can Provide Required Conductivities as Insulators/Dielectric Materials. (B)-(D) Scanning Electron Microscope (SEM) Images for Carbonized Cotton Candy, Cotton, and Silk, Respectively. (E) Conductivity Spectrum of Food- Based Materials that Can Cover a Wide Range of Electrical Conductivity from Conductors to Insulators. (F)-(G) SEM Images for Broccoli Powder and the Cross-Sectional View of the Edible Piezoelectric Thin Film Consisting of Gelatin and Broccoli Powder.	12
Figure 2.6 Characterization of the Piezoelectric Performance of (A) Commercial PZT Film and Films Which Were Made with (B) Broccoli, (C) Cabbage and (D) Cauliflower. Besides Broccoli/Gelatin Piezoelectric Thin Films, Cabbage and Cauliflower as the Active Materials in the Piezoelectric Thin Films Are Also Made Using the Same Procedures.....	17
Figure 2.7 Results of Food-Based Electrical Components. Optical and SEM Images Are Shown, Along With the Characteristics of the Components. (A) Wires; (B) Resistors; (C) Inductors; (D) Capacitors.....	20
Figure 2.8 (A) Images of Wires with Different Au Coating Time, 1, 5 and 10 Mins. (B) Resistance Test Result of Wires with Different Coating Time.....	21
Figure 2.9 Resistance Test Result of Resistors With Different Composites. Resistors with Different Composites Were Made to Get a Wide Range of Resistance. Carbonized Silk and	

Carbonized Cotton Candy Were Used as a Substitute for Carbonized Cotton. The Content of Carbonized Silk and Carbonized Cotton Candy Was Controlled at 10%, 20% and 30%.	21
Figure 2.10 Performance of Inductors with Different Diameters Under Frequency Range From 103 to 106 Hz.	22
Figure 2.11 Properties of Capacitors with Different Composition Under Frequency Range From 103 to 106 Hz.	23
Figure 2.12. Photograph And Illustration of the Edible Piezoelectric Microphone and the Characterization Procedure of the Edible Microphone.....	23
Figure 2.13. Recorded Voltage Waveform Showing Fidelity of the Recorded Sound Using Edible Microphone.	24
Figure 2.14. Amplitude of the Input Abdominal Sound and Amplitude of the Recorded Abdominal Sound.	24
Figure 3.1 (A) Photograph of pH Sensor Version 1, (B) Illustration of pH Sensor Version 1.....	27
Figure 3.2 Illustration of the Working Principal and Detection Scheme of the pH Sensor.....	29
Figure 3.3 Characterization of the Edible pH Sensor In Solutions with pH Value from 1 to 12	30
Figure 3.4 Eudragit's Dissolving Process in a Base Environment of pH 9.....	31
Figure 3.5 Capsules' Dissolving Rate vs. Content of Eudragit.....	31
Figure 4.1 Photograph of pH Sensor Version 2	33
Figure 4.2 Structure of the pH Sensor Version 2	33
Figure 4.3 Illustration of the Planar Pattern of an Inductor for a Typical pH Sensor.....	37
Figure 4.4 Illustration of a Rolled Inductor.....	38
Figure 4.5 Simulation or Different Topologies of Rolled Inductors.....	39
Figure 4.6 Schematic of Testing Inductance	40
Figure 4.7 pH Sensor's Frequency vs. pH in Relative to Additional Capacitor	42
Figure 4.8 A More Complex Model of an Inductor.....	43
Figure 4.9 Revised Pattern Version 1 for Inductor	44
Figure 4.10 Testing Circuit for Rolled Inductor.....	45
Figure 4.11 Transient Response for Measured and Simulated Data	46

Figure 4.12 Cut Pattern to Measure Parasitic Capacitance of the Rolled Inductor.....	47
Figure 4.13 Revised Pattern Version 2 for The Rolled Inductor.....	48
Figure 4.14 Revised Pattern Version 3 for The Rolled Inductor.....	49
Figure 4.15 Two Version of Patterns for Single-Line Inductors.....	50
Figure 4.16 Comparison of Inductance Between Rectangular Patterned Inductor and Non- Rectangular Patterned Inductor.....	51
Figure 4.17 New Pattern of the Improved pH Sensor	52
Figure 4.18 Schematic of Testing Bench for the Reading Circuit.	54
Figure 4.19 Signal Comparison Between High Input Power and Low Input Power.	56
Figure 4.20 Simulated Mutual Inductance vs. Distance Relative to Different Inner Diameter of the Planar Coil.	58
Figure 4.21 Signal Strength of an Artificial pH Sensor Vs. Frequencies at Different Distances. ..	59
Figure 4.22 Signal Strength of a Real pH Sensor vs. Frequencies at 2cm Distance.....	60
Figure 4.23 The Setup for Testing the pH Sensor with a Handheld Device.	61
Figure 4.24 The Testing Result From the Handheld Device After Testing a pH Sensor In a Solution of Hydrochloric Acid with A pH Value 3.....	62
Figure 4.25 Voltage-Frequency Response of the pH Sensor in a Solution of Hydrochloric Acid with a pH Value 3 Recorded From the Handheld Device.....	63

CHAPTER 1

1 INTRODUCTION

Innovations of medical technologies and devices such as glucose monitors, heart rate monitors, nerve stimulators have significantly helped doctors to diagnose and treat diseases, which helps patients keep healthy and prolong their lifespan [1]. Medical devices are classified to diagnostic equipment like medical imaging machines, treatment equipment like infusion pumps, life support equipment to maintain the function of the patients, medical laboratory equipment, medical monitors that measure the patient parameters including electrocardiography, electroencephalography, and blood pressure.

Implantable devices have a significant role in the healthcare monitoring, diagnosis and therapy. Cardiovascular medical devices are implanted to treat conditions such as cardiac arrhythmia, and heart failure. Such devices include implantable cardioverter-defibrillator, and cardiac pacemaker. Electrical implants embedded in the neck of patients are used to relieve pain from rheumatoid arthritis, where electrical signals are sent to vagus nerve. Bioactive implants are used to deliver drugs when oral route of drug delivery is not suitable. Surgeries and medical procedures are required to implant the devices into human body, and if a battery replacement is required or the end of lifetime of the device has reached, another surgery or procedure for the patients is needed. Such surgeries and medical procedures are relatively expensive, potentially giving financial burdens to patients and the process of recovery after the surgeries and procedures introduces risks to other infections and other side effects.

Biodegradable electronics such as transistors, batteries and sensors are proposed as the materials used are within the safe dose of allowance. Iron (Fe), tungsten (W) and molybdenum (Mo) are biodegradable metals for the substitute of traditional conductive materials like copper and aluminum. Biodegradable materials like Ecoflex made from potato and corn starch are used as insulative substrates. Inorganic materials like silicon and silicon dioxide degrades in the body safely and thus serve as semiconductor materials and insulative materials. Once the biodegradable devices are implanted in the body, they degrade by body fluid or blood at a

controllable rate while remaining harmless. The usage of biodegradable electronics as implantations eliminates the necessity of surgeries to take the device out of the body, which reduces the cost for the patients and potential risks of infections and other side effects.

In the recent decades, the electrical capsules that are implanted into human body by swallowing came into the market [2-5]. Wireless capsule endoscopy consisting of a camera in the capsule takes photos in the gastrointestinal (GI) tract and sends images to an external receiving device. "Smart" capsules with sensors and circuits inside the encapsulation measure the temperature, pressure, acceleration and pH value within the GI tract [6-10]. These swallowable devices do not need surgeries during operation giving more convenience and eliminating risks induced by surgeries.

Although the electrical capsules have merits for point of cares, they have a chance to get stuck in the intestinal, where another procedure must be taken to get it out from the anal, which is incontinent to the patients, and such procedure brings additional cost to the patients. Besides, the capsules consist of toxic materials like copper-based circuits and batteries, resulting severe damages to organs once leaked. Thus, edible or digestive electronics where the whole devices are made from food and other edible materials are studied to form a new solution for testing of medical parameters in the GI tract.

The next chapter demonstrated a food kit for edible materials and electrical components were fabricated and tested, along with some applicable devices, such as microphones and acidity level (pH) sensors. The development and optimization of pH sensors and related testing circuits were carried out in the following chapters.

CHAPTER 2

2 FOOD BASED EDIBLE AND NUTRITIVE ELECTRONICS

2.1. Background and Motivations

Implantable electronics are useful and, in some scenarios, essential to maintain patients' life, such as cardiac devices and drug delivering systems [11]. While the surgeries or procedures for the implantations have potential risks for the patients, including bleeding and infections. At the end of the lifetime of such implantable medical electronics, an additional surgery or procedure is required to take the products out of human body, resulting more cost for patients and additional potential risks.

A more biocompatible device having less chances of harming human bodies is preferred. To achieve more biocompatibility, biodegradable electronics are studied such as biodegradable transistors and interconnects [12-15]. These devices are either entirely or partially degradable and the degrading materials are within safe dose of acceptable materials regulated by American Food and Drug Administration (FDA). Another way with more biocompatibility is achieved with electronics directly contacting surfaces of the human body, through skins, GI tract et al. Human skins are naturally protective for the body from harsh environment, giving more capabilities for medical electronics to contact with to monitor health status and treat disease. For example, an Apple watch monitors heart rate constantly and feedbacks potential underline medical conditions whenever an abnormal of behavior of heart rate is detected [16-18].

GI tract has a large surface area that allows medical electronic devices to monitor a broad range of parameters. Swallowable capsule-based devices monitor the temperature, pressure, pH to help doctors to diagnose diseases while surgeries and procedures are not required for the functions of these devices, thus eliminating the potential risks to the patients. Although swallowable capsule-based medical devices lower the medical bill compared with implantable devices, they suffer from the risks of retentions and leakages, while a portion of patients get the capsules stuck within the GI tract after swallow and potential leakages of the electrical devices when still inside of GI tract are poisons to patients, leading to more health risks.

Edible, digestible and absorbable devices would further advance the field as they contact directly with surface area of GI tract and have less risks while degrading, though require advances in materials, beyond initial efforts. The present study uses basic natural food materials to form fundamental electrical components and devices, giving building blocks of edible and digestible integrated circuits for further integration and more functions of medical electronics.

The study starts with a screening of a broad range of food that are safe. The methodology behind this is that food is what people eat for thousands of years and are proven to be selected for consideration of safety and nutrients. Most food is organic material and consists of different composites like cellulose and water, thus difficult to characterize the electrical and mechanical properties for general usage in the electronics. So, a process is developed to dry and ground the food material to test with, and further categorized into different types of materials in terms of electrical and mechanical performances. For example, vegetables are rich in water, and dried vegetables have low conductivity and thus useful for insulative materials for electronics. Carbonized cottons are relatively conductive compared to insulative materials like oil.

After classification of food-based materials in terms of the conductivity and dielectric constant, a food kit or “cookbook” is developed for creating electrical components in integrated circuits. For example, rice paper, sugar powder, flour and rice are capable of functional as structural materials for substrates of printed circuit board (PCB). Metal traces on top of the substrate form electrical interconnects for the PCB. The food kit is used to make discrete electrical components like wires/interconnects, resistors, inductors and capacitors. Other components like antennas and simple circuits are demonstrated in the following study.

While developing the food kit for electrical components, piezoelectric effects of cellulose-rich materials like broccoli and cabbages are found and studied for their piezoelectric properties. An edible piezoelectric microphone is developed based on the piezoelectric phenomenon of broccoli, though the piezoelectric parameter is relatively smaller than commercial materials like lead zirconate titanate (PZT).

2.2. Experimental Section

2.2.1. Preparation of the Materials

Dried food: Each vegetable/fruit was cut into round slices with thickness of 1 to 2 mm and diameter of 1 to 4 cm. A household food dryer was used to dry vegetable/fruit slices under 60 °C for 12 h.

Carbonized cotton candy, cotton and silk: Cotton candy/cotton/silk were annealed at 280 °C for 1 h at a heating rate of 2 °C /min, and subsequently annealed at 1000 °C for 1 h at a heating rate of 6 °C /min in an argon flow. Then the carbonized cotton candy/cotton/silk were grinded into small pieces (about 0.3mm in diameter) in a mortar.

Piezoelectric composite thin films: A gelatin/broccoli film works as piezoelectric film. Gelatin (2 g) was sprinkled over the distilled water (20 g). Leave the mixture for 10 min for the gelatin to fully swell. Then gelatin solution was prepared by dissolving gelatin in distilled water under magnetic stirring for 30 min. The temperature was controlled at 60 °C. Broccoli powder (0.5 g) and glycerol (1.2 g) were added into gelatin solution and stirred for 10 min. Gelatin/broccoli films were produced by solution casting on acrylic glass plate at 50 °C for 12 h.

2.2.2. Preparation of Shadow Mask

The pattern of the mask was designed in AutoCAD and was transferred into a Mylar film (0.1 mm in thickness) using a laser cutter (VLS 6.60 laser cutter, Universal Laser System, Inc.). The laser cutter would cut through the Mylar film to make a shadow mask.

2.2.3. Preparation of Electrical Components

(1) Wire/interconnects

The edible wires/interconnects consisted of a substrate and a layer of conductive trace. The substrate was made of rice paper or any other food-based material that has resistivity larger than $1 \times 10^{10} \Omega \cdot \text{m}$. The dimension of rice substrate was 3 mm \times (20-50 mm) \times 0.2 mm (thickness). A shadow mask with interconnects" pattern was attached to the rice paper using egg white as the adhesive layer. Interconnects were dried in oven at 70 °C for 8 h. The substrate was

then placed in a vacuum chamber of gold sputtering machine, where gold was deposited on the substrate through the shadow mask, with thickness of 100 nm.

(2) Resistor

Sweet potato starch (1.5 g), active charcoal (0.45 g) and carbonized cotton candy (0.5 g) were mixed in a ceramic container and grinded for 10 min to make them uniformly dispersed. The container was then put on a hotplate (200 °C) and heated for 5 min, followed by adding distilled water (2 g) and heating for another 5 min under constant stirring. Now the mixture forms a low-viscous dough. The mixture was then transferred into a syringe. Syringe with different sizes of orifice can be used and in fact the size of the orifice defines the diameter of the edible resistors. The typical diameters are 2 mm. The mixture was pushed out with the rate of 0.7 mL/min into boiled distilled water for 3 min and then immersed in the distilled water of room temperature to make them more tenacity. Finally, the sample was put into an oven and dried at 60 °C for 12 h. The edible resistors are basically conductive and edible noodles. Carbonized cotton and silk can be similarly used to replace cotton candy. Flour can also be used to replace sweet potato starch in this process.

(3) Inductor

The edible inductors were made by following the similar procedure of making edible resistors. After the mixture was pushed into the boiled distilled water and immersed in the distilled water of room temperature, the sample was wined around a cylindrical object (e.g., a tube). The winding length and diameter define the inductance. The typical diameters are 2 mm and the length ranges from 40 to 80 cm. Then, they are dried in an oven with 60 oC for 12 h. Finally, after the sample was completely dried, it was taken off from the cylindrical object.

(4) Capacitor

A gelatin film was used as the dielectric layer. Gelatin (2 g) was sprinkled over the distilled water (20 g). Leave the mixture for 10 min for gelatin to fully swell. Then gelatin solution was prepared by dissolving gelatin in distilled water under magnetic stirring for 30 min. The

temperature was controlled at 60 °C. Glycerol (1.2 g) was added into gelatin solution as plasticizer and stirred for 10 min. Gelatin films were produced by solution casting on acrylic glass plate at 50°C for 12 h. The typical thickness of the by a shadow mask. Two same shadow masks were attached to gelatin film's both sides with carefully alignment. Gold was deposit for 200 nm thickness on both sides using gold sputter. The shadow masks were removed after deposit and the capacitor was just made.

(5) PCB board

Each edible PCB board substrate consists of powdered sugar, xanthan gum and egg white. Powdered sugar (60 g), xanthan gum (0.5 g) and egg white (12 g) were mixed in a glass bowl by hand mixer. Keeping mixing them until a sticky paste was achieved and most of the powdered sugar was incorporated. Additional powdered sugar (20 g) and the sticky paste were poured on the workbench. Kneading them until a smooth and non-sticky dough was formed. The sugar paste dough was divided by 8 pieces. Each of them was rolled out and cut into a 7 cm × 7 cm × 0.2 cm piece, followed by drying at room temperature for 12 hrs. Before placing shadow mask on substrate, a uniform egg white layer was coated on the surface of substrate. Egg white will make the surface adhesive to have a good connection with shadow mask. Substrate will be ready to be deposited gold against a shadow mask after drying it in oven at 70 °C for 8 h.

(6) Antenna

The shadow mask is made using the same method described previously. Then the shadow mask is attached to the PCB board substrate, followed by gold deposit using gold sputter for 200 nm. The shadow mask is removed after deposit and the antenna is made.

2.2.4. Preparation of Samples for Mechanical Test

The same procedure was followed to prepare sweet potato starch dough, powdered sugar dough, and flour powder dough. All the dough was kneaded and cut into a plate with dimension of 3 × 2 × 0.2 cm for the mechanical test. The Instron 4411 was used to perform the compression test.

2.2.5. Characterization of Materials, Components, And Devices

(1) Conductivity characterization

Potentiostats (Gamry Potentiostats Reference 300) and multimeter (hp Hewlett Packard) were used for raw and dried food materials. For powdered food material: A stainless steel mold with 1-inch in diameter was used to hold the powder food material, including fresh milk powder, carbonized cotton candy/cotton/silk, all-purpose flour and sugar powder. Then 30 MPa pressure was applied on the mold to achieve a condensed tablet. Two stainless steel plates were placed on two sides of food material tablet to form a “sandwich” structure for electrical conductivity measurement (Figure 1.1) using Gamry Potentiostats Reference 3000. For liquid food material, a plastic box with copper foils on two sides (Figure 2.2) was used to hold the liquid food material. Then two copper foils were connected to multimeter for the resistance measurement.



Figure 2. 1 “Sandwich” structure for electrical conductivity measurement

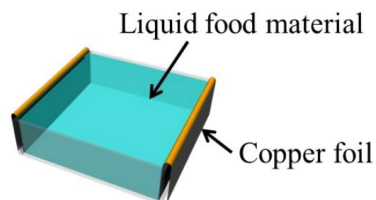


Figure 2.2 Sample holder for electrical conductivity measurement for liquid materials.

(2) Capacitance measurement

It was measured on probe station with precision LCR meter (Hewlett-Packard 4061A semiconductor/component test system).

(3) Inductance measurement

The dimensions are measured with caliper and the inductance was measured by the same equipment for the capacitance measurement.

2.2.6. Mechanical Characterization of Food Materials as Structural Functions

The sample is placed on the platform of the tool material test system (Instron 4411) for compression test. After initial setup, compressive force through a pressing target is loaded and recorded as well as the displacement of the pressing target until failure of the sample. The first few data are used to calculate the Young's Modulus. The stress is calculated by dividing force by top area of the sample, and the strain is calculated by dividing displacement and thickness of the sample. Then the Young's Modulus is calculated by dividing stress by strain.

$$E = \frac{\sigma}{\varepsilon}$$

$$\sigma = \frac{F}{a}$$

$$\varepsilon = \frac{\Delta l}{l}$$

2.2.7. Characterization of the Piezoelectric Coupling Coefficient

(1) d_{33} : Sample's dimensions, weight and capacitance were measured before the test. The schematic of the characterization is shown in Figure 2.3, where a beam was fixed at an end and the other end was attached to an electric shaker. The sample was attached onto the beam at the 3/4 of distance to the end of the shaker by wax and an accelerometer was mounted at the same location to measure the acceleration of the sample. The electric shaker was connected to its power supply and a signal generator with frequency of 50 Hz. During the vibration applied by the shaker, the inertia force was applied to the sample via $F = ma$, which generates a voltage V at the sample that was characterized by a signal analyzer. Thus, the piezoelectric coefficient d_{33} is calculated by $d_{33} = \frac{CV}{F}$, where C is the capacitance of the sample that was characterized separately.

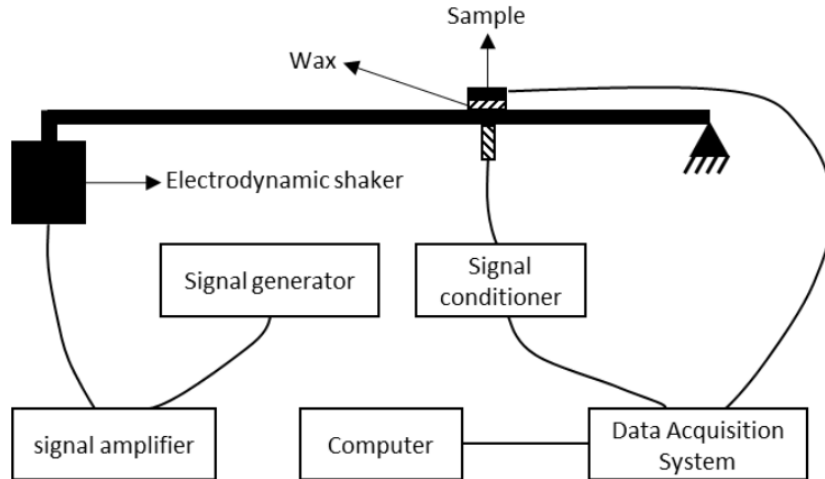


Figure 2. 3 Schematic of the characterization of d_{33} .

(2) d_{31} : d_{31} was characterized by a fatigue load frame (Bose ElectroForce Biodynamic 5160) and current was measured with a picoammeter (Keithley 6485) (Figure 2.4 (a)). The samples were prepared with 8x25.4mm Ag paint electrodes in top and bottom surfaces, and the electrodes were then extended with Cu tape to allow a proper connection with the picoammeter (Figure 2.4 (b)). Dynamic force was applied on the sample to measure periodic output current.

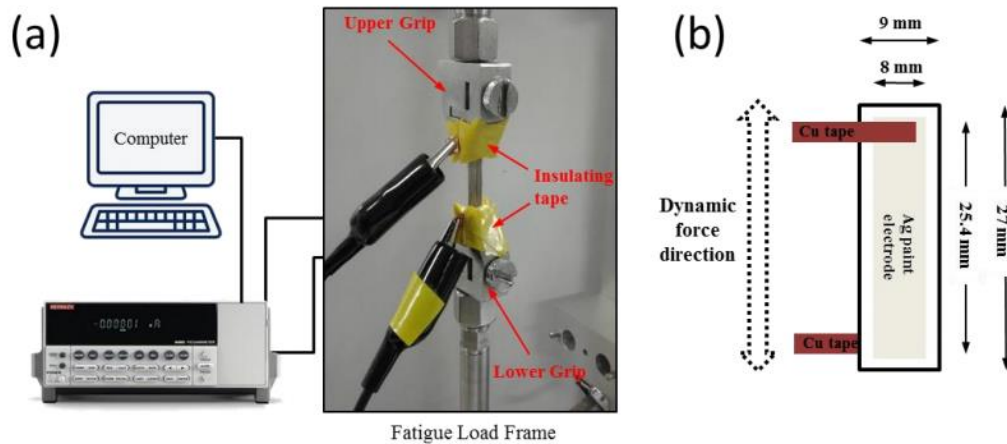


Figure 2. 4 (a) Equipment set up for characterization of d_{31} . (b) Sample and electrode design.

2.3. Result and Discussion

In the present study, natural foods and foodstuffs were chosen as candidates for electronics materials and then based on specification requirements identified additional edible processed foods, food components, and on a limited basis nontoxic levels of electronic materials, to create full electronic constructs. The best candidates from natural, processed, and adduct food materials were then selected to create the “preferred food kit” for component fabrication. Specific individual and combined components were built and characterized utilizing the preferred food kit. The present study significantly enables edible electronics with the potential to advance an emerging domain of biomedical technologies and devices.

As a first step, reference materials were selected to establish the specifications needed for components. Electronic components require insulators and conductors, which can be specified by their electrical conductivities. For insulators (or dielectric materials), the conductivity is lower than 10^{-8} S/m; while it needs to be larger than 10^6 S/m for conductors. The insulators are used to build encapsulations and as the dielectric materials in capacitors with the capacitance in the typical range of 1 pF-100 nF. The conductors appear in wires/interconnects, electrodes and other components. Mixed insulators and conductors can be used to build resistors with a wide range of resistance from 10 Ω -20 M Ω . Those reference values establish the specifications needed for components and devices fabrications using food materials.

As a second step, specific natural, unprocessed foods were selected, organized according to recognized, defined nutritional food groups from the Food Guide Pyramid (e.g., cereals, meat, vegetables, bread, fats, etc.), as candidate materials for analysis due to their electrical properties and subsequent component or device fabrication. Conductivity probes and semiconductor parameter analyzer were used to perform the characterizations (see details in Methods). As seen in Figure 2.5 (a) for electronic conductivities, oils and dried foods (including meat, vegetables, gelatin, fruits, and bread) that are shaded achieve required conductivities as insulators/dielectric materials. Here gelatin was cataloged into meat as it is derived from collagen in animal raw materials. The dried foods were made using a typical food dryer. The reason of

being good insulators is that those foods are covalent components and do not contain mobile electrons to conduct electric current. On the contrary, foods that contain salts (e.g., butter) and water (e.g., fresh meat and vegetables) are relatively conductive because of the presents of free ions to conduct electric current.

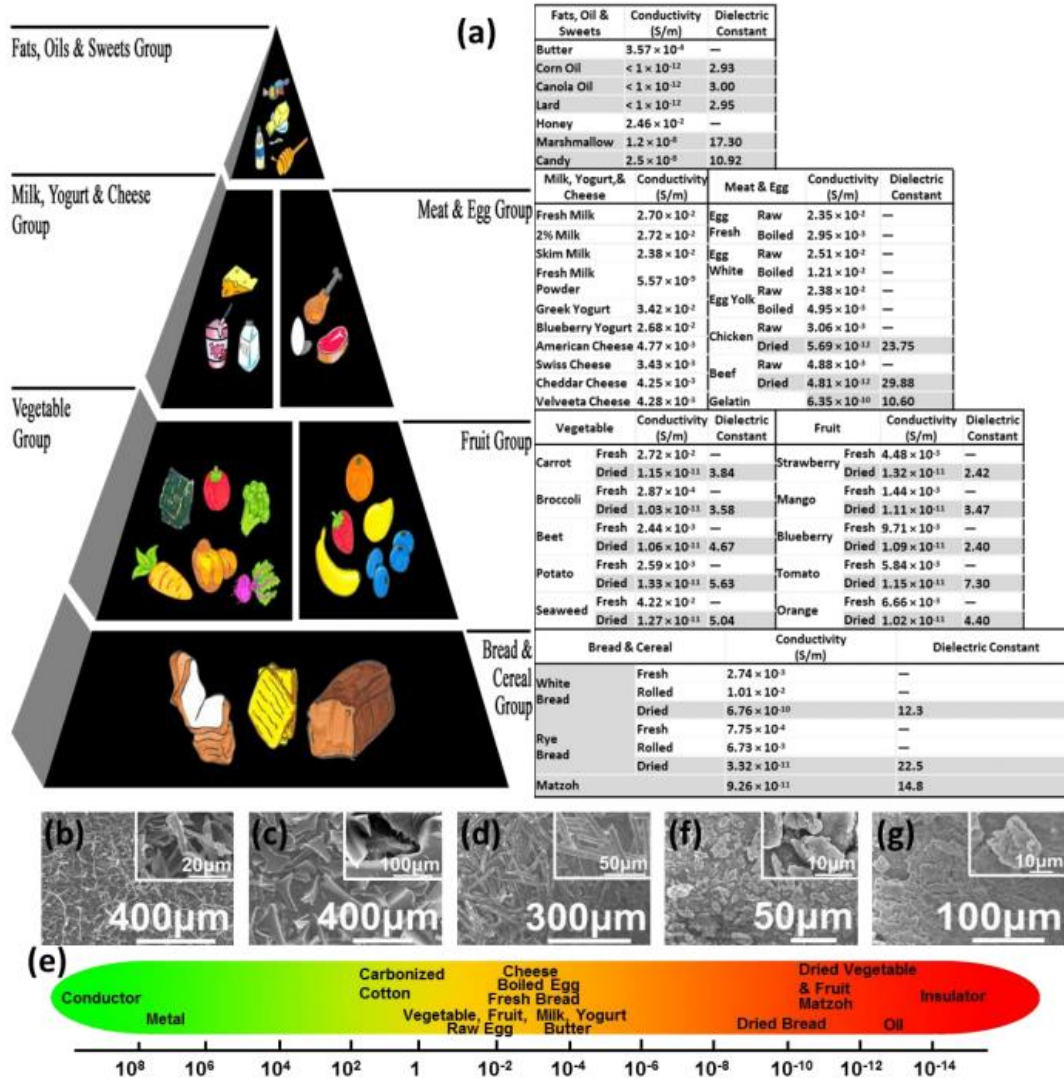


Figure 2. 5 Selections and characterizations of food-based materials regarding their electrical properties. (a) A typical food pyramid with conductivities and dielectric constants of some representative food materials according to recognized food groups. The shaded elements represent food materials that can provide required conductivities as insulators/dielectric materials.

(b)-(d) Scanning electron microscope (SEM) images for carbonized cotton candy, cotton, and silk, respectively. (e) Conductivity spectrum of food-based materials that can cover a wide range of electrical conductivity from conductors to insulators. (f)-(g) SEM images for broccoli powder and the cross-sectional view of the edible piezoelectric thin film consisting of gelatin and broccoli powder.

A more comprehensive list of electrical conductivity and dielectric constants of commonly accessible food materials were provided in Table 2.1. Figure 2.5 (a) apparently shows that nature foods can provide good insulators/dielectric materials but not good conductors for electrical components. In order to fill the gap in conductivity to create full constructs in electronic components, processed foods and non-toxic levels of electronic materials were identified. In addition to edible metals as conductors, carbon derived from processed foods, basically, activated charcoal, carbonized sugar (cotton candy), cellulous (cotton), and protein (silk) were selected and tested. Annealing process was used for carbonization (see Methods). The energy dispersive X-ray spectrometry (EDX) results show that they are actual carbon. (see Figure 2.6). Different microscale morphologies of carbonized cotton candy (Figure 2.5 (b)), cotton (Figure 2.5 (c)), and silk (Figure 2.5 (d)) as observed in the scanning electron microscope images attribute to different electrical properties. Specifically, the fiber-like carbonized cotton tends to form a continuous path to conduct electron while the flake-like carbonized cotton candy and silk have to aggregate to form the similar conductive path.

Table 2.1 Comprehensive list of conductivity of commonly accessible food materials

Food materials	Conductivity (S/m)	Dielectric Constant
Fats, Oil & Sweets	Gummy Bears	—
	Chewing Gum	23.10

	Sugar	2.58×10^{-9}	9.53
	Glucose	1.01×10^{-9}	4.78
	Dextrose	1.40×10^{-9}	5.26
	Molasses	7.14×10^{-4}	—
	Karo Syrup	1.25×10^{-3}	—
Meat & Egg	Chicken (Cooked)	9.43×10^{-4}	—
	Beef (Cooked)	4.74×10^{-4}	—
Vegetable	Guar Gum	5.2×10^{-9}	9.99
	Xanthan Gum	8.43×10^{-10}	16.30
	Kale (Fresh)	6.42×10^{-6}	—
	Kale (Dry)	2.25×10^{-11}	6.58
	Cauliflower (Fresh)	3.11×10^{-5}	—
	Cauliflower (Dry)	2.04×10^{-11}	4.97
	Cucumber (Fresh)	8.83×10^{-4}	—
	Cucumber (Dry)	0.86×10^{-11}	5.37
Fruit	Banana (Fresh)	4.79×10^{-3}	—
	Banana (Dry)	1.12×10^{-11}	6.00

	Pineapple (Fresh)	1.75×10^{-3}	—
	Pineapple (Dry)	1.38×10^{-11}	4.56
	Avocado	2.48×10^{-3}	—
Bread & Cereal	Flour	5.67×10^{-10}	6.32
	Corn Starch	2.93×10^{-10}	7.95

The electrical conductivity results given in Table 2.2 show that these processed food materials and non-toxic metals can serve as the conductive materials. It is apparent from Figures 2.5 (a)-(d) and Table 2.1 and 2.2 that edible food materials can cover a wide range of electrical conductivity as shown in the conductivity spectrum Figure 2.5 (e). To build a conductive wire/interconnect, edible metals are good choices while dried vegetables mixed with bread/flour and oil are good candidates for insulators. The mixed carbonized cotton candy and flour can be used to build resistors.

Table 2.2 Conductivity of processed food materials

Processed Food	Conductivity (S/m)
Carbonized Cotton	35.07
Carbonized Cotton Candy	22.46
Carbonized Silk	28.29

In addition to insulators and conductors in electrical components, other functional materials are also indispensable, particularly for sensing. For example, piezoelectric materials can generate electricity upon mechanical stress and have been used in many applications including pressure sensors, microphones and speakers. Many nature and edible materials have

piezoelectric effects, such as bones and tendons. Cellulose that is rich in many vegetables (such as broccoli and brussels sprouts) also has piezoelectric effects. The mechanism is that the oriented cellulose crystallites in these vegetables exhibit shear piezoelectricity due to the internal rotation of polar atomic groups associated with asymmetric carbon atoms. Here broccoli powder with radius less than 90 m was used to mix with gelatin to form a piezoelectric composite. SEM images show the broccoli powder (Figure 2.5 (f)) and a cross-sectional view of the edible piezoelectric thin film (Figure 2.5 (g)). Broccoli powders (Holistic Herbal Solutions, LLC) they uniformly mixed with gelatin solution through magnetic stirring followed by casting under room temperature. The stiffness of the thin film can be tuned by adding edible plasticizer glycerol (see Methods). The piezoelectric coupling coefficients of the edible piezoelectric thin film were characterized by using electric shaker, accelerometer and signal analyzer (see Methods). They are $d_{33} = 4.3 \text{ pC/N}$, and $d_{31} = 0.31 \text{ pC/N}$. These values are comparable to 5 pC/N of ZnO. In addition to broccoli that is rich in cellulous, other cellulousrich foods, including brussels sprout and cabbage were also mixed with gelation to form piezoelectric composites using the similar approach. The same characterization approach was used, and the results are given in the Fig 2.6. It is concluded that they all exhibit appreciable piezoelectric effects.

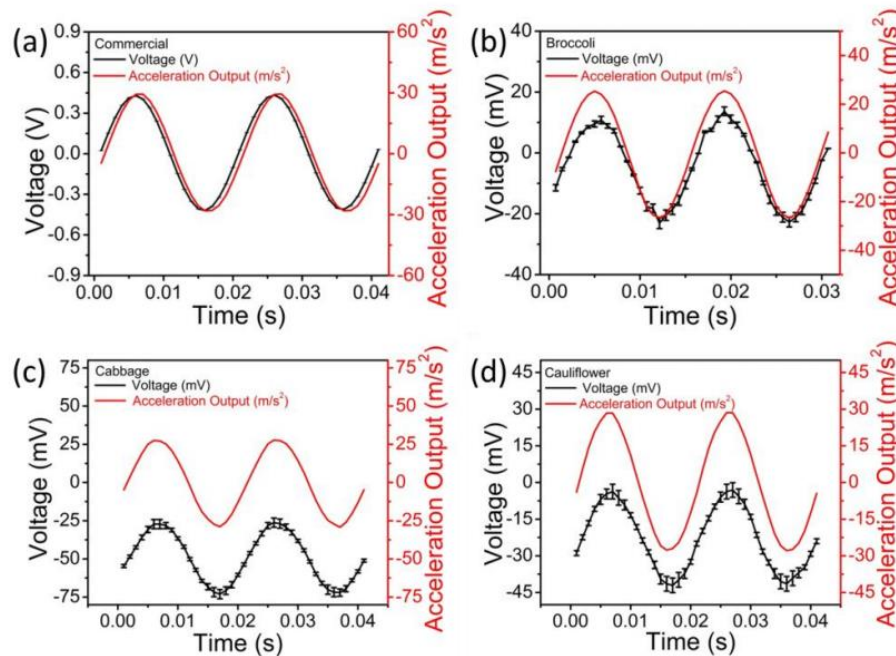


Figure 2. 6 Characterization of the piezoelectric performance of (a) commercial PZT film and films which were made with (b) broccoli, (c) cabbage and (d) cauliflower. Besides broccoli/gelatin piezoelectric thin films, cabbage and cauliflower as the active materials in the piezoelectric thin films are also made using the same procedures.

Under the same weight ratio between cellulous containing vegetables and gelatin, broccoli has the strongest piezoelectric effects since it is the most cellulous-rich vegetables. It should be noted that gelatin also has detectable piezoelectric effects since it is derived from collagen in animal raw materials. However, its d_{33} is about 30 times less than that of broccoli (Table 2.3).

Table 2.3 D_{33} of different piezoelectric materials

Piezoelectric materials	D_{33} (pC/N)
Commercial PZT	550
Pure gelatin film	0.185
Broccoli/gelatin film	4.3
Cabbage/gelatin film	0.66
Cauliflower/gelatin film	3.00

The studies of food materials with respect to their electrical properties opens opportunities to build a toolkit for necessary electrical components, as shown in Table 2.4. The food materials in the toolkit are grouped into structural and electrical functions. Insulative food materials, such as sweet potato starch, sugar powder, and flour, basically provide structural functions. Distinct applications of these materials in electrical components attribute to their

different mechanical properties (e.g., elastic modulus and bending rigidity). Specifically, rice paper is very thin and thus very flexible so that it is used as the substrate in wires/interconnects. Though both sweet potato starch and flour can be used as the substrate in resistors and inductors, a dough of sweet potato starch is easy shaped and tends not to fracture at the dried state, compared with regular flour. The reason is that sweet potato starch contains more starch than flour, and starch will gelatinize in the presence of water and heat. After gelatinization, starch dough will become uniform and sticky which makes it easy to be shaped into desired shapes with smooth surface. Thus, sweet potato starch can serve as a good substrate for resistors and inductors. The conductive food materials, such as edible metals and carbonized cotton candy, contribute to the electrical functions. The wires/interconnects need to have very small electrical resistance so that edible metals are used; while for resistors, carbonized cotton and cotton candy that have relatively low electrical conductivity are used. To achieve good adhesive between the substrate and conductive regions, egg white was used as the binding materials if necessary. The presence of hydrogen bonds and ionic interactions with proteins attribute high adhesive strength and allows egg whites as good adhesive materials. The components in Table 2.4 were built using the suggested food materials.

Table 2.4 A toolkit using food-based materials to build necessary electrical components.

Component	Food Kit Materials	
	Structural Function	Electrical Function
Wire	Rice paper, sugar powder, wheat flour, rice	Gold leaf, edible metal: gold
Resistor	Sweet potato, sugar powder, wheat flour, hard candy, dried fruit, vegetable	Active charcoal, carbonized cotton fiber / cotton candy / silk, gold leaf

Inductor	Sweet potato powder, wheat flour, hard candy, dried fruit, dried vegetable	Active charcoal, carbonized cotton fiber / cotton candy / silk, gold leaf
Capacitor	Gelatin, dried fruit, dried Vegetable	Gold leaf, edible metal: gold
Antenna	Sugar powder, wheat flour, rice paper, hard candy, marshmallow, egg white	Edible metal: gold, gold leaf, active charcoal, carbonized cotton /silk

The optical microscopy and SEM images along with the characterization results are shown in Figures 2.7. The edible wires are made of rice paper as the substrate and sputtered Au as the functional part. The thickness of the Au is on the order of 100 nm (Figure 2.7 (a)). The resistors and inductors are all made of sweet potato starch and carbonized cotton candy through an extrusion process using a syringe, where the resistors are straight wires (or basically conductive “noodles”) and the inductors are winded against a cylindrical object (or basically noodle-based spring). Another layer of carbonized cotton was added on the outside of the noodles while they are still wet to increase the conductivity. As shown in the SEM images in Figure 2.7(b), carbonized cotton forms a continuous path in the noodles. The capacitors are made of thin gelatin sheets as the dielectric layers coated with edible Au as the electrodes. The Figure 2.7 (d)). By adding glycerol as the plasticizer and a high-k material in gelatin, the mechanical flexibility and effective dielectric constants can be improved. A plasticizer could reduce the glass transition temperature (T_g) and increase the plasticity of the material. Glycerol as a common plasticizer is widely used in the pharmaceutical field, such as softening the capsule and biomedical or biodegradable materials.

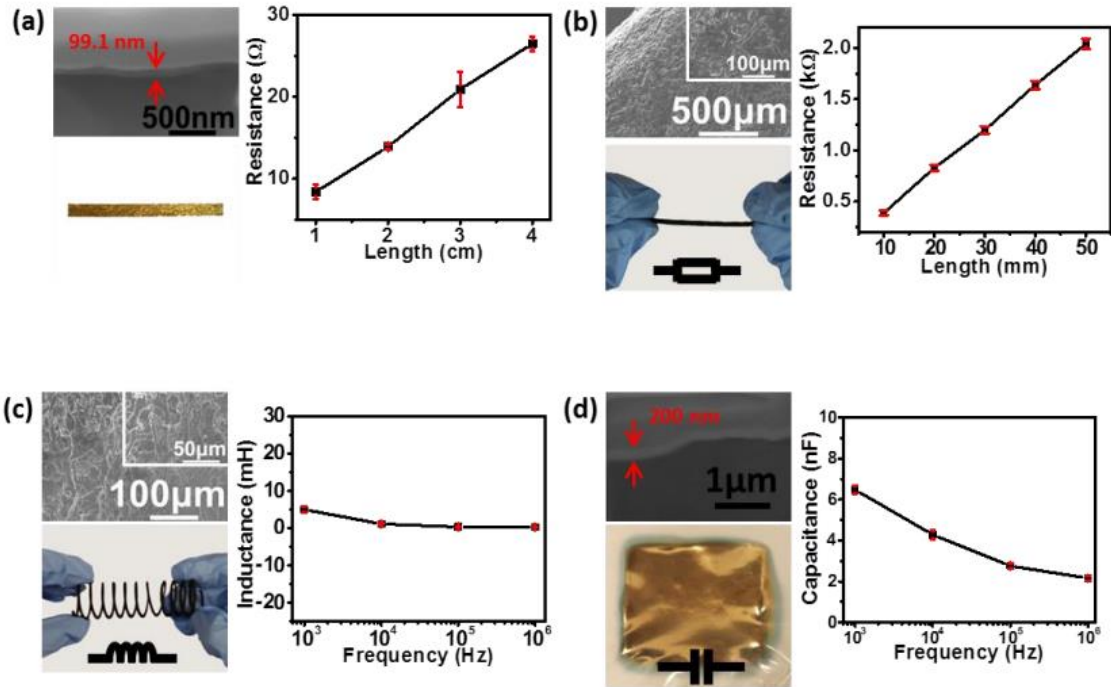


Figure 2. 7 Results of food-based electrical components. Optical and SEM images are shown, along with the characteristics of the components. (a) Wires; (b) Resistors; (c) Inductors; (d) Capacitors.

In addition to the food materials presented in Figures 2.7, more food materials have been used to build these components. Similar characteristics have been achieved as shown in the Figure 2.8-2.11. It is thus convincing that edible food materials can build functional circuits.

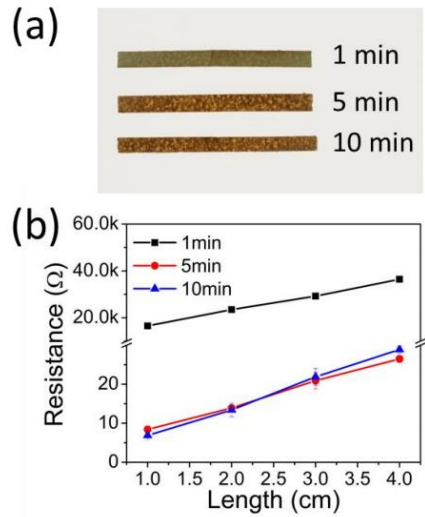


Figure 2. 8 (a) Images of wires with different Au coating time, 1, 5 and 10 mins. (b) Resistance test result of wires with different coating time.

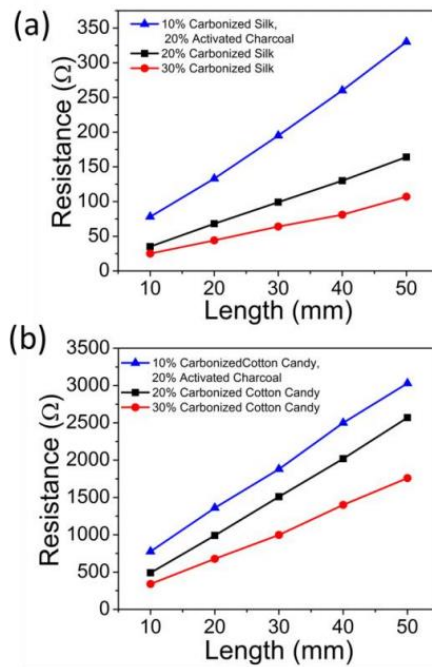


Figure 2. 9 Resistance test result of resistors with different composites. Resistors with different composites were made to get a wide range of resistance. Carbonized silk and carbonized cotton candy were used as a substitute for carbonized cotton. The content of carbonized silk and carbonized cotton candy was controlled at 10%, 20% and 30%.

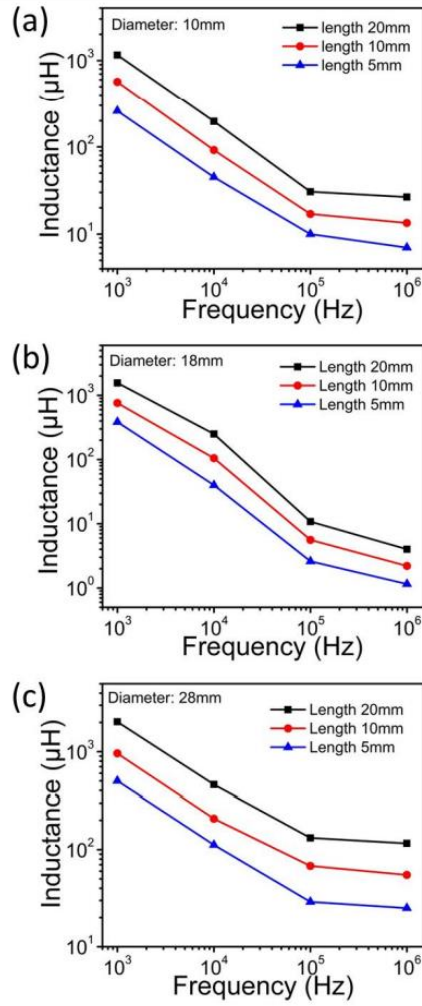


Figure 2. 10 Performance of inductors with different diameters under frequency range from 103 to 106 Hz.

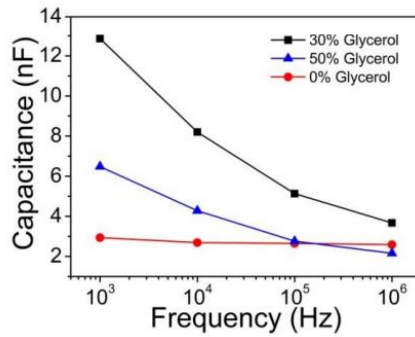


Figure 2. 11 Properties of capacitors with different composition under frequency range from 103 to 106 Hz.

To demonstrate that the edible piezoelectric thin film can be used to convert mechanical vibration to appreciable voltage changes for potential biomedical applications, an edible piezoelectric microphone was built, in which a 2 mm thick edible piezoelectric thin film was coated with 200 nm thick Au electrodes on both sides (Figure 2.12).

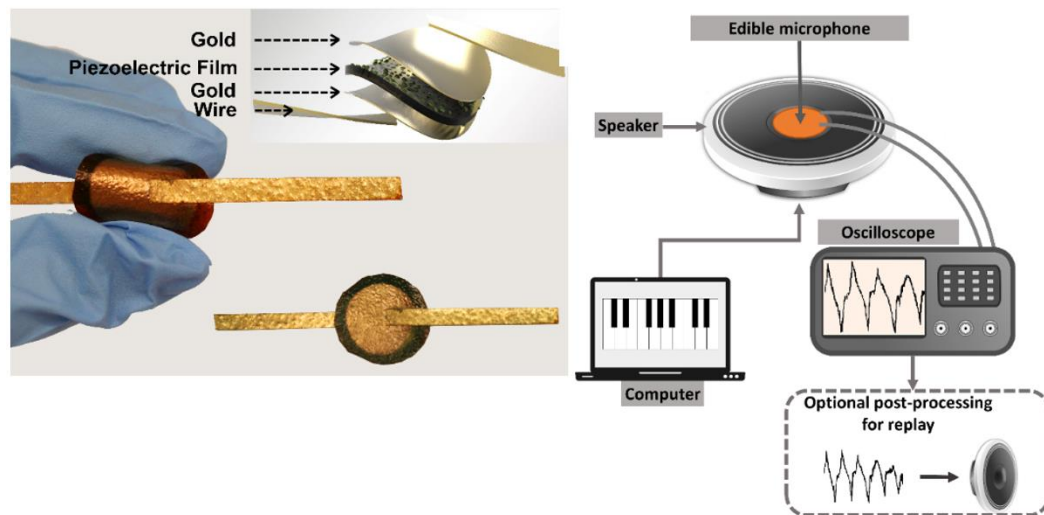


Figure 2. 12. Photograph and illustration of the edible piezoelectric microphone and the characterization procedure of the edible microphone.

To test the edible microphone, a sound with defined frequency generated from a computer (i.e., virtual piano keys) was played back via a loudspeaker where the edible microphone was firmly attached to the loudspeaker diaphragm to detect the mechanical vibration, with the edible microphone was connected to an oscilloscope to record and show the voltage waveform. The recorded analog voltage signals from the oscilloscope were further fed to a loudspeaker for optional playback. Specific frequencies (ranging from 27 to 131 Hz) generated by the virtual piano keys (e.g., A0, C3) through a computer program matched very well with the recorded voltage waveform (Figure 2.13), demonstrating that the edible microphone can record fidelity sound. It is noted that the waveform in Figure 2.13 represents averaged response so that the peaks are not evenly distributed.

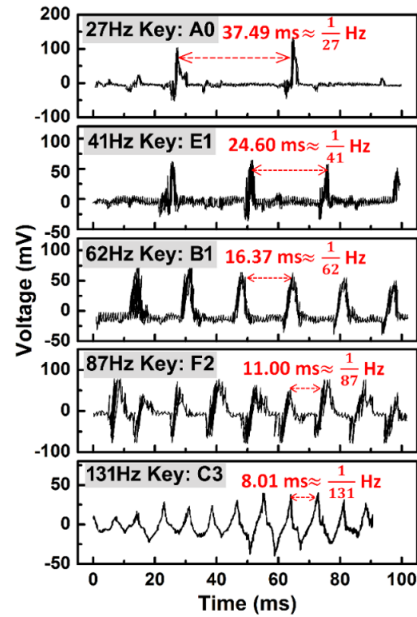


Figure 2. 13. Recorded voltage waveform showing fidelity of the recorded sound using edible microphone.

Low-frequency sound is particularly important in biomedical applications as it is within the range of abdominal associated with both normal and pathologic conditions. To demonstrate the biomedical application, bowel sounds from a 70-year-old man with abdominal pain were fed to the loudspeaker and recorded via the edible microphone (Figure 2.14). It was observed that the recorded voltage waveform successfully reproduced the original testing sound.

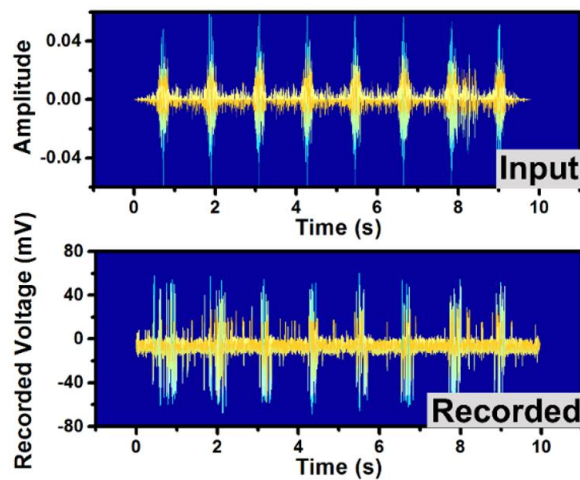


Figure 2. 14. Amplitude of the input abdominal sound and amplitude of the recorded abdominal sound.

CHAPTER 3

3 EDIBLE WIRELESS PH SENSORS: VERSION 1

3.1. Background and Motivation

A lot of people suffer from diseases with GI tract like stomachache and gastroesophageal reflux. Traditional diagnosis methods use tubes inserted into the stomach, which is inconvenient and sometimes painful for the patients. In the recent decade technique like capsule endoscopes (PillCam™, Medtronic, Minneapolis, MN) can detect pH values, temperatures within one pill [19-25]. These devices are not biodegradable and have the risk of causing bowel obstructions if they become entrapped in areas of stenosis, where another procedure must be taken to get them out. Besides, these capsules are not safe if the non-edible materials used in the ingestible electronics leak into human body.

Real-time measurement of pH values in the GI tract has significant medical importance. Patients with acid secretory disorders (gastroesophageal reflux disease, peptic ulcer disease, Zollinger-Ellison syndrome) would benefit from regular intermittent monitoring of gastric pH particularly if this could be done inexpensively and safely [26-36]. In the present study, a pH sensor was constructed and tested. The present study significantly enables edible electronics with the potential to advance an emerging domain of biomedical technologies and devices.

In the previous chapter, a new class of electronic materials derived predominantly from natural foods and foodstuffs, with minimal levels of inorganic materials, was developed to build edible electronic components, and such components were capable to be integrated together to have a whole electronic device or system. An edible and digestive pH sensor was proposed to encounter these problems above for its biocompatibility and the sensor breaks down in the intestinal with only a small portion of the manufacturing cost.

3.2. Mechanism of the Edible pH Sensor

The working mechanism is that for acidic solutions, the H⁺ ions reside at the electrodes making the capacitance of the electrodes dependent on the concentrations of the H⁺ ions, which is the pH value of the solution. The pH sensor has a coil as an inductor, forming an inductor-capacitor circuit along with the electrodes. The first version of edible pH sensor consists of gold-zinc oxide (Au–ZnO) as working electrodes, an antenna made of Au for wirelessly transmitting signals, and an edible capacitor, and a substrate made from sugar paste.

The reaction of ZnO with either acidic or basic solutions (Acidic: $ZnO_{(s)} + H_s^+ \Leftrightarrow Zn(OH)^+$, basic: $ZnO_{(s)} + 2H_{(2)}O \Leftrightarrow Zn(OH)_3^- + H_s^-$), resulted in a change in the capacitance (C) between Au and ZnO electrodes, and thus the resonant frequency of the pH sensor changed with the pH value via $f = \frac{1}{2\pi\sqrt{LC}}$, where L is the inductance of the antenna that does not depend on the pH value. A reading circuit sweeps frequency and detect the signal reflection of the pH sensor. At the resonant frequency of the pH sensor, the reflected signal has a strongest strength, which corresponds to the capacitance of the electrodes, and the pH value of the solutions.

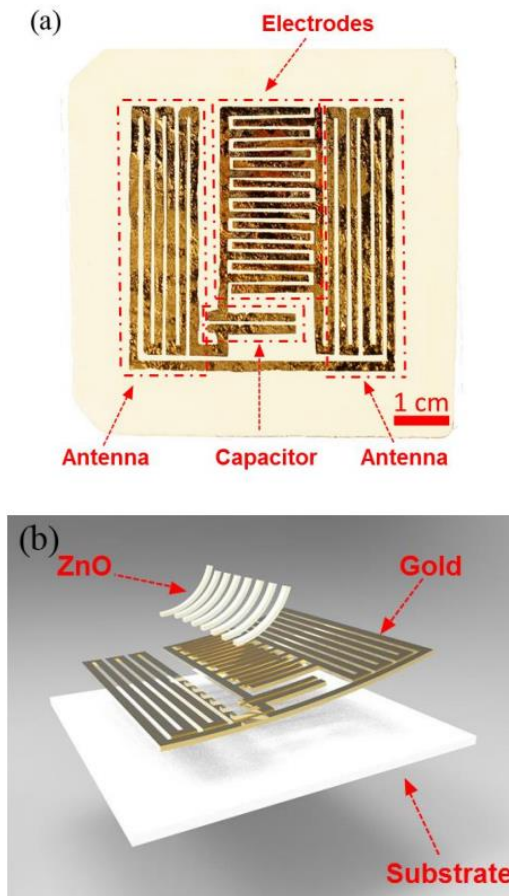


Figure 3.1 (a) Photograph of pH sensor version 1, (b) Illustration of pH sensor version 1

3.3. Experimental Section

3.3.1. Fabrication of the pH Sensor

The pattern of the mask was designed in Solidworks and was transferred into a sheet metal (0.5 mm in thickness) using a technique of electric discharge machining. The electric discharge melted the metal and along with the patterned route the shadow mask was made.

Each substrate consists of powdered sugar, xanthan gum and egg white. Powdered sugar (60 g), xanthan gum (0.5 g) and egg white (12 g) were mixed in a glass bowl by hand mixer. Keeping mixing them until a sticky paste was achieved and most of the powdered sugar was incorporated. Additional powdered sugar (20 g) and the sticky paste were poured on the

work bench. Kneading them until a smooth and non-sticky dough was formed. The sugar paste dough was divided by 8 pieces. Each of them was rolled out and cut into a 7 cm × 7 cm × 0.2 cm piece, followed by drying at room temperature for 12 hrs. Before placing shadow mask on substrate, a uniform egg white layer was coated on the surface of substrate. Egg white will make the surface adhesive against a shadow mask after drying it in oven at 70 °C for 8 hrs.

The substrates of pH sensor were then placed in a vacuum chamber of gold sputtering machine, where gold was deposited on the substrate through the shadow mask, with a thickness of 200 nm. Finally, the shadow mask was removed.

The surface with antenna and capacitor pattern was coated by 1mm thick Eudragit L100 coating solution which was made in the preparation of substrate step using solution using spraying coating technology and dried for 5 min. Then a second layer of Eudragit L100 coating was coated in the same way. The gelatin coating solution was prepared by dissolving gelatin (2 g) into distilled water (10 g). The surface of sample with electrodes pattern was coated by 1mm thick gelatin coating solution using spraying coating technology and dried for 1 h.

The remained Eudragit L100 coating solution was put into oven and dried at 80 °C for 10 min to form a sticky and glue-like solution. The sample was rolled onto stainless steel stick (4 mm in diameter) which will be draw out later to form a cylinder shape. During rolling, the surface with gold pattern faced outside and the end with antenna was rolled first. Finally, the end of the sample with electrodes was stick to itself using the glue-like Eudragit L100 solution.

3.3.2. Characterization of the pH Sensor

A reading circuit shown in Figure 3.2 sweeps frequency and detect the signal reflection of the pH sensor. At the resonant frequency of the pH sensor, the reflected signal has a strongest strength, which corresponds to the capacitance of the electrodes, and the pH value of the solutions.

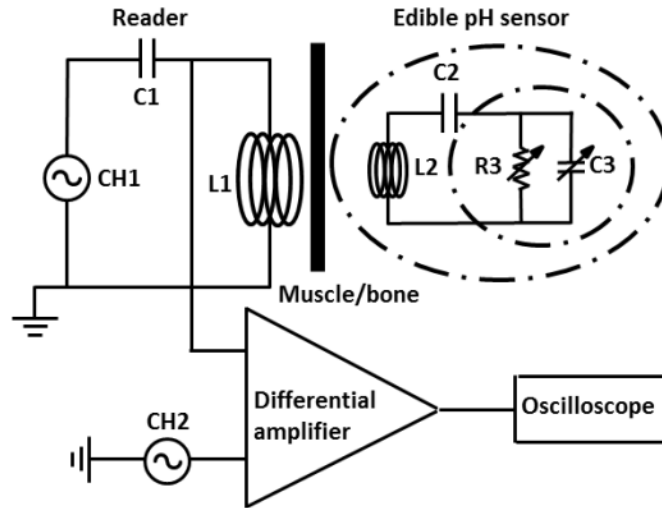


Figure 3.2 Illustration of the working principal and detection scheme of the pH sensor

3.4. Result and Discussion

To validate and calibrate the edible pH sensor, the pH values of reference solutions were measured via a standard pH meter (Hanna Instruments); the capacitance of the Au–ZnO electrodes were characterized utilizing a probe station with precision LCR meter (Hewlett-Packard); and the resonant frequency of the pH sensor was detected by a circuit consisting of a reader, a differential amplifier, a signal generator, and an oscilloscope (Figure 3.3). In the calibration, the edible pH sensors were immersed in the standard solutions with pH values from 1 to 12. As shown in Figure 3.3, the capacitance varied with the pH values. Based on the measured pH-dependent capacitance C , the resonant frequency of the pH sensor was calculated using $\frac{1}{2\pi\sqrt{LC}}$, where $L = 0.45 \mu\text{H}$ and was separately measured. It is apparent that the calculated resonant frequency agreed very well with the measured values. Our results demonstrate that the edible pH sensor was able to measure the pH value of solutions that are both acidic and basic.

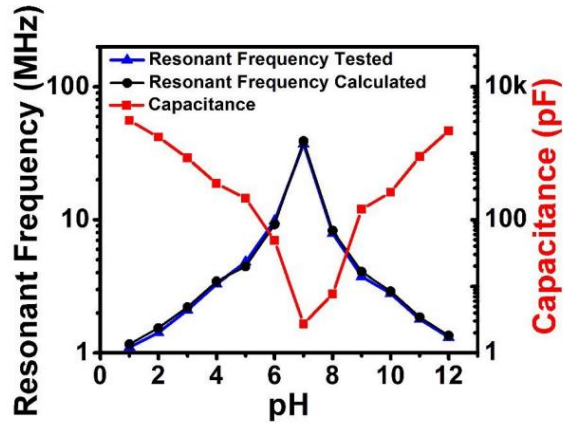


Figure 3.3 Characterization of the edible pH sensor in solutions with pH value from 1 to 12

In the practical application, patient needs to swallow the pH sensor through throat into gastrointestinal tract. In the next study, the overall structure and pattern of conductive circuits are also re-designed delicately to deduce size so that it can be swallowed easily. Gastric residence time is another important factor that determines the value of the swallowable pH-sensor. Typically, the gastric residence time varies from a few minutes for liquids to a few hours for proteins and fats. Therefore, the ability to control the digestible time of the substrate of the pH sensor was studied. The materials of encapsulation layer and substrate are modified so that the digestive time can be precisely controlled.

The reason to use Eudragit is it does not dissolve in acid solutions but does in base solutions. Once the pH sensor is swallowed into stomach, the capsule will not dissolve because of the protection of Eudragit. After the pH value of the stomach is tested, the sensor will go to intestines where the environment is base. Eudragit encapsulation will dissolve in the base environment and open the rolled sensor, thus accelerating the degrading process. Figure 3.4 shows the dissolving process in a base environment of pH 9.

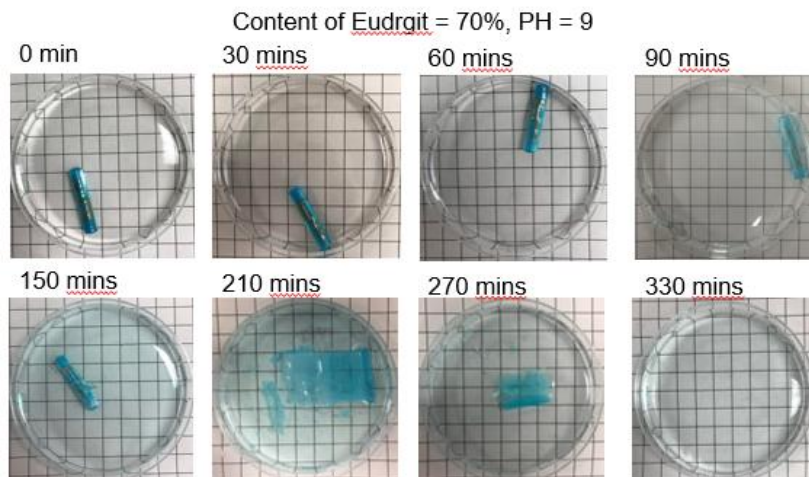


Figure 3.4 Eudragit's dissolving process in a base environment of pH 9.

Mixing different mass ratios of Eudragit leads to different dissolving rate the film, where the dissolving rate can be tuned as shown in Figure 3.5. At pH 9, the dissolving time decreases when the content of Eudragit goes high, from about 300 minutes when the ratio is 40% to about 50 minutes when the ratio is 100%, and it is because Eudragit dissolves in basic solution and the rest of the contents do not dissolve as fast as Eudragit in the same basic environment. Depending on the requirement from the practical usage, the dissolving rate is tuned with respect to the content of Eudragit.

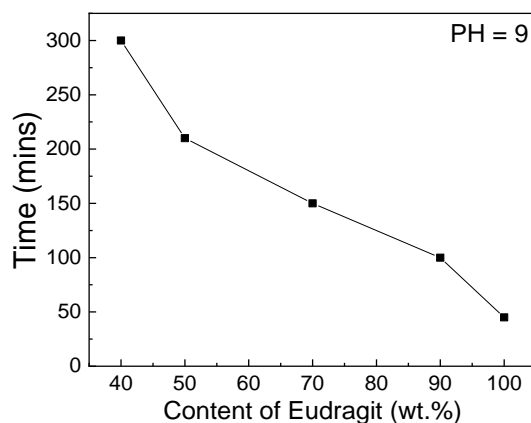


Figure 3.5 Capsules' dissolving rate vs. content of Eudragit.

CHAPTER 4

4 EDIBLE WIRELESS PH SENSORS: VERSION 2

4.1. Introduction

In the last chapter the edible pH sensors were demonstrated with its biodegradable merits and low cost compared with other electrical capsules. However, the form factor is too large to swallow and the fabrication of a large area of gold dominates the cost of production. A new design of the pH sensor was demonstrated in this chapter to accommodate the issue with form factor, making the whole device practical for patients to swallow like a capsule.

Another benefit from this new design of the edible pH sensor is the low cost compared to other commercial devices that are used with a capsule shape. The commercial devices are fabricated with silicon based integrated circuit, connected with other components including metal traces, discrete electrical components, batteries on to printed circuit boards. And the whole device is encapsulated with hard material for protection of the functional circuit. All that fabrication process is relatively expensive compared with the edible pH sensor when the commercial devices are massively produced in a factory.

Although the edible pH sensor proposed in this chapter has less functionalities than the commercial ones that measure the temperature, pH value, acceleration in the GI tract, the innovated edible pH sensor has a digestive property that allows the sensor to dissolve in the intestine of human body after it passes through the stomach, which makes the edible pH sensor has a lower chance of retention compared with the commercial devices. It is more convenient to the patients along with the doctors as less issue to deal with in the hospital, where no more medical procedures are required once retention happens.



Figure 4.1 Photograph of pH sensor version 2

The photograph of the pH sensor is shown in Figure 4.1, where the yellow part is the gold trace protected with gelatin films that are transparent. The interdigit parts are electrodes and cover the outer surface of the capsule rolled from a planar film shown in Figure 4.2.

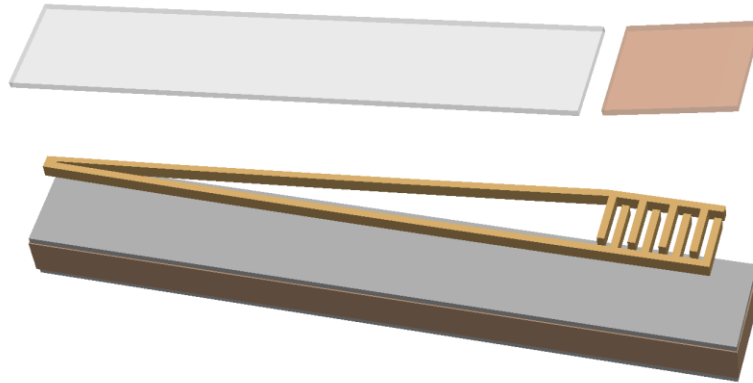


Figure 4.2 structure of the pH sensor version 2

New design of gold circuit was deposited on the surface of Eudragit L100 substrate by sputtering machine. Then the antenna and capacitor circuit parts were coated with Eudragit L100 coating to protect them from stomach fluid. The electrodes' part was coated with gelatin coating to protect it from rub and push in the stomach. The gelatin coating swelled and absorbed stomach fluid as soon as it contacted with the stomach fluid. Finally, the substrate was rolled into a cylinder with 22mm length and 5mm diameter. Thus, the resonant frequency of the pH sensor changed with the pH value according to the equation $f = \frac{1}{2\pi\sqrt{LC}}$, where L is the inductance of the antenna that does not depend on the pH value. The pH - resonant frequency of the pH sensor version is shown in Figure 3.11.

The development of the electrodes is in section 4.2, where the range of the capacitance is designed and optimized in the favor of the frequency bandwidth and resolution so that the detecting setup could successfully pickup the signals within its operating bandwidth. Then, the inductor is designed in terms of overall dimensions, rolling angles, metal trace's width to make the inductance as large as possible but still in compliance of a 6-inch semiconductor fabrication standard. More insights going into the design of the inductor show that the quality factor plays a significant role in terms of the signal strength in mid-range distance, while resistance of the inductor needs to be as small as possible to achieve a large quality factor. One way is to increase the thickness of the metal trace but doing so increases the cost of fabrication. More designs are made to pursue the high quality factor by decreasing the resistance and even though by sacrificing a little amount of inductance. Further study shows the bandwidth of the pH sensor is too large for the handheld device to cover, so a large parasitic capacitance is proposed in parallel to the electrodes, making the total capacitance of the pH sensor goes up but with a smaller ratio of bandwidth. Doing so makes the pH sensor compatible to the handheld device from a third party company. After the designs of the pH sensor and the development of the handheld device from the vendor, fabrications are demonstrated in section 4.4 and the characterization is done in section 4.5.

4.2. Design of Electrodes


The electrodes act as the sensing part of the pH sensor, where capacitances of electrodes change in terms of the acidic level of the environment. The frequency bandwidth is determined by $f = \frac{1}{2\pi\sqrt{LC}}$, where the range of the capacitive change of the electrodes significantly affects the bandwidth. The sensitivity of electrodes comes with the resolution of capacitances in response to different acidic environment. From the doctors' input, most patients' pH level in the stomach ranges from 1 to 6, which would be the range of detection from the electrodes. Then, because the acidic level of the stomach has a one-to-one relation to the capacitance of the electrodes, the objective is to engineer the range of the capacitance of the electrodes to cover the acidic levels needed to be tested. Theoretically, the larger range of the capacitance, the more



resolution of the pH value. However large capacitive range results to wide bandwidth for the sensor along with the reading circuit, giving more technique challenges to develop the wide bandwidth reading circuit. The design of electrodes needs to be optimized to achieve the range of the reading bandwidth as well as the resolution needed for detection.

To achieve the tunes of capacitance of the electrodes, the total width and length, electrodes' width and the gap between electrodes are the key parameters, as the geometry defines the overall surface area of the electrodes for detection to form the two conductive sides of the capacitor. And the distance or gap between electrodes is the effective distance for the capacitor. An ideal capacitor's capacitance is $C = \epsilon A/d$, where ϵ is the permittivity of the material, A is the active area for each electrode, and d is the distance between two electrodes. Although the electrodes used in the pH sensor is more complex with multiple interdigits as electrodes, the total capacitance of the pH sensor follows the principal of capacitive theory. The total width complies with the overall length for the rolled pH sensor, which follows the guidelines of the allowable size for capsules. For example, for a size 00 capsule, the length of it is 23.4mm. For the size of 000 capsule, the length could be 26mm.

Given consideration of the key parameters of the pH sensor, a few versions of electrodes are designed as shown in Table 4.1 and the resulting capacitances are listed within the table.

Table 4.1. Conductivity of processed food materials

Electrode version	Preview	C (pF) at pH1	C (pF) at pH6	Electrode gap (mm)	Electrode width (mm)	Total width (mm)	Total length (mm)
1		3550	39	0.4	0.4	14.74	16.67

2		10000	260	0.6	1	24.8	18.7
3		6300	363	1	1.5	23	18

The length of the electrodes' pattern must be within the outer perimeter of the pH sensor to prevent overlapping of the electrodes. Otherwise, some part of the electrodes would be covered by the outer layer of the electrodes, making the covered area inactive to sense. During the rolling process of the inductor, accuracy of rolling is considered to accommodate the electrodes' covering area, so that whenever the under rolling or over rolling happens in the fabrication, all the electrodes are exposed to the air and not overlapped to achieve the full functionality of sensing in the testing environment.

4.3. Design of Inductor

The initial design of the inductor for the pH sensor is a coil-like inductor rolled from a planar pattern shown in Figure 4.3. The pattern is fabricated with the same method of previous pH sensor, with gold deposition through a shadow mask to a substrate. The substrate is the sandwiched structure where Eudragit-gelatin/glycerol-Eudragit films are formed and after the deposition of gold, the inductive area is covered with Eudragit material by spray coating of Eudragit solution dissolved in ethanol. Ethanol will evaporate leaving the Eudragit film on to the gold trace and the substrate to protect the gold from cracking.

If the gold cracks by any mishandling, the circuit will break and result in a failure of fabrication. The yield of the pH sensor highly depends on the uniformity of the gold trace and a partial crack in any cross section of the gold trace would bring the resistance of the inductor higher and the quality factor of the inductor will suffer because of the increased resistance.

Another way to prevent the gold trace's defect is to improve the flexibility of the films, making the total rolling process easy to conform along the bar that is rolled on. Glycerol is a good candidate material to increase the plasticity of the composite resulting more flexibility of the film. In comparison, Eudragit material is rather brittle and fragile when rolled or bent. There are two ways to increase the flexibility of the film, one is to add glycerol to Eudragit solution dissolved in ethanol, and the other one is to make the coating film thin. A study is made to tune the mass ratio of Eudragit, glycerol and ethanol for a high flexibility enough to roll well along a 4-mm bar without cracking the gold trace inside. The spray coating thickness would affect the thickness of the coating film thus needs to be controlled to achieve a relatively good flexibility.

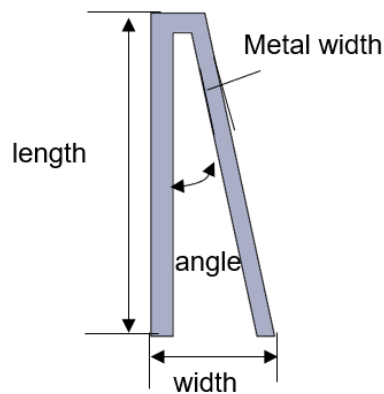


Figure 4.3 Illustration of the planar pattern of an inductor for a typical pH sensor

After it rolls beginning from the top part along with a metal bar with a diameter of 4mm, the rolled pattern aligns with its left edge shown in Figure 4.3, to get a rolled pattern shown in Figure 4.4. Precautions are made to prevent the gold trace from cracking and the alignment of the left side of the pattern must be controlled to form a planar inductor in the left part. The Eudragit-gelatin/glycerol-Eudragit film is relatively transparent so alignment is easy to make with bare eyes.



Figure 4.4 Illustration of a rolled inductor

The key parameter for the performance of an inductor is the quality factor $Q = L/(wR)$, where L is the inductance, R is the resistance of the inductor, and w is the angular frequency. A high-quality factor contributes to a high signal strength. To achieve this objective, a large inductance and low resistance is desired.

A few designs of inductors are simulated in COMSOL, with different folds of initial designs. The modeling of the simulation consists of a 10cm long of planar pattern, with a thickness of 800nm, and a trace width of 1mm. Given the fixed overall boundaries from the guideline of capsules, one to four folds of designs are modeled with material gold. The simulated inductances are shown in the Figure 4.5, along with the quality factors. Note that the radical frequency is taken as 10MHz for the simulation. As shown in the figure, more repeated patterns in a compact space have larger inductances, but suffer from having lower quality factors, mainly because of the faster increase of resistance. In the following, the planar pattern with only on fold is optimized in terms of other parameters.

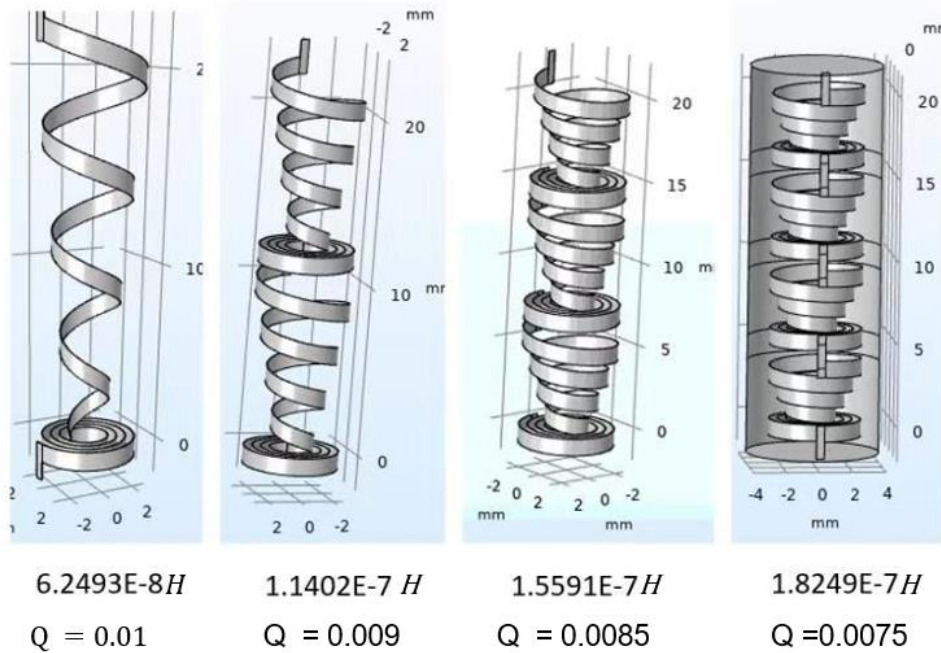


Figure 4.5 Simulation of different topologies of rolled inductors.

The pattern's angle, width, length, and metal-trace width all affect the performance of the inductor. Further experiments were done to optimize the inductance of the pH sensor, shown in Table 4.2. It is observed that the longer the length is, the larger the inductance is, while increasing the metal-trace width would decrease the inductance. However, the longer length of the pattern leads to a larger area of fabrication. The deposition of metal is carried out in a sputtering equipment where it is in compliant with semiconductor manufacturing process, where the equipment is considered an expensive capital tool. Usually, the sputter provides substrate at a range of maximum dimension of 2 inches, 4 inches, 6 inches, 8 inches and 12 inches. The larger the chamber of the sputter supports, the more expensive the equipment is. Mainstream semiconductor sputter has a supporting dimension of 6 inches in diameter of the substrate, which is the typical limit for the pattern of the pH sensor, where the length of the inductor adding with the length of the electrodes, should not exceed about 6 inches. More advanced factories use 8 inches and 12 inches for the supporting dimension to accommodate the corresponding sizes of the wafers.

Table 4.2 Inductances with different length, width, and metal-trace width

Inductance (μH)	Length (cm)	Width (mm)	Metal-trace width(mm)
0.25	14	20	1
0.19	10	20	3
0.23	13.5	20	5
0.3	14.4	20	5
0.35	14.5	20	4
0.4	15	20	4
0.52	16	20	4
0.6	16	20	3

The inductance is measured from a LCR meter and verified with a testing circuit shown in Figure 4.6. A spectrum analyzer with a tracking generator sends out a sweeping signal to the testing inductor, a standard capacitor with a known capacitive C value and feeds back to the spectrum analyzer's input port, forming a LC circuit with stimulus and responsive measurement. The resonant frequency f is recorded in the spectrum analyzer and the inductance L is calculated from $L = \frac{1}{4\pi^2 f^2 C}$.

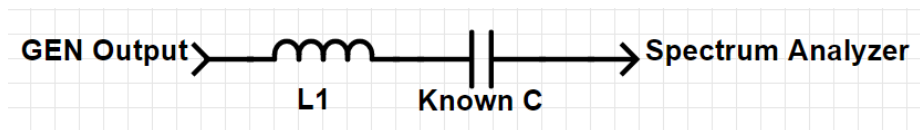


Figure 4.6 Schematic of testing inductance

The angle of the planar pattern is also studied to optimize the inductance of the pH sensor. According to Table 4.3, angle 4.5° has the highest inductance. Further analysis shows that it is the angle that has the highest inductance when the rolled metal trace does not overlap and has no gaps in the lateral view.

Table 4.3 Inductances with different angles

Inductance (μH)	Angle ($^\circ$)
0.182	2
0.2036	2.7
0.211	3.3
0.2138	4
0.21421	4.5
0.21418	4.7
0.21413	4.8
0.2140	5
0.2136	5.5
0.2131	6

While realizing mobility of the testing bench with superior range of detection from the new handheld device, more constrains related to the development of the pH sensor are considered. For example, the handheld device has a function of auto scanning and calibration with a limited range of bandwidth, which is about 2 to 3 times from the lower bound to the higher bound of the

operating bandwidth. The pH sensor's bandwidth (from about 4MHz to about 40MHz) has 10 times of ratio between the lower bound to the higher bound, making the handheld device difficult to cover the whole range of frequency. To solve the problem, an additional capacitor needs to be added to lower down the bandwidth, shown in Figure 4.7. With an additional capacitor in parallel with the electrodes, the frequency response of the improved sensor is shown in the Figure 4.7. According to the figure, with 100pF added to the capacitance, the frequency's upper bound is as low as about 21MHz, which is a significant improvement to the bandwidth of the pH sensor. With 500pF of additional capacitance, the bandwidth's frequency ratio could be lower into a range of 2 to 3 times, which is practical for the handheld device to test.

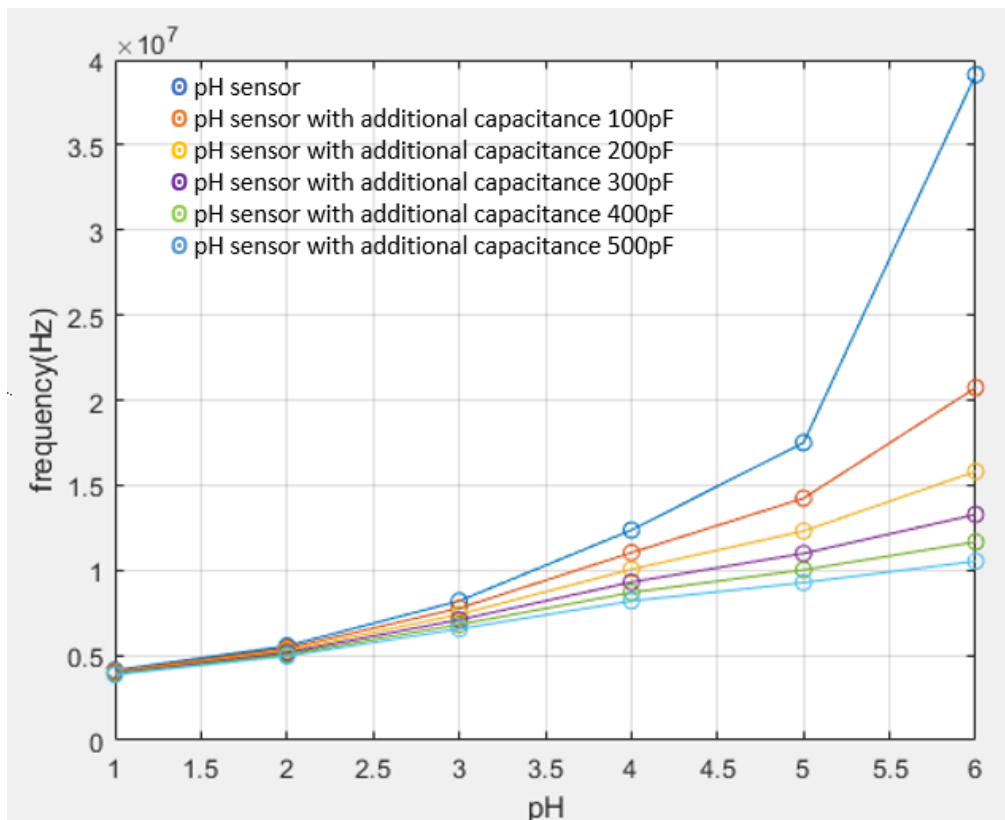


Figure 4.7 pH sensor's frequency vs. pH in relative to additional capacitor

Further study of the additional capacitor to the pH sensor was done by adding more parasitic capacitance to the rolled inductor of the pH sensor. A more complex model of an inductor is introduced including a parasitic capacitance that is large enough to not ignore, where a

real inductor consists of an ideal inductor in series of a resistor and then in parallel with a capacitor, shown in Figure 4.8. The parasitic capacitance is in parallel with the electrodes when the rolled inductor is connected to the electrodes. The total capacitance would be the addition of the capacitance of the electrodes and the parasitic capacitance of the rolled inductor. The increased total capacitance leads to a lower resonant frequency of the sensor and a lower frequency bandwidth.

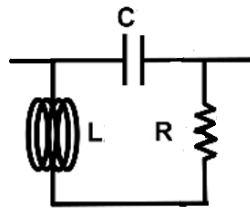


Figure 4.8 A more complex model of an inductor

To get a relatively large parasitic capacitance for the rolled inductor in the pH sensor, one method is to decrease the thickness of the substrate, making the capacitor's plates closer to each other. By reducing the mass of the materials in the step of substrate fabrication, the thickness of the substrate is decreased to about 90 μ m. The other method is to increase the permittivity of the substrate. The substrate consists of three major types of material, gelatin, glycerol and Eudragit, along with some water residues due to fabrication process. Glycerol and Eudragit have larger permittivity than gelatin. By playing around the ratios of material, an overall permittivity is increased, resulting in a large parasitic capacitance shown in Table 4.5. Note that the planar pattern for the rolled inductor is a rectangular shape with a length of 12cm and width of 4mm.

Table 4.5 Parasitic capacitance of rolled inductor.

Thickness of substrate (μ m)	Capacitance (μ F)
150	390

To increase the additional parasitic capacitance of the inductor, revised patterns are made for comparison for the inductor. Figure 4.9 shows a revised version of inductive pattern that increase the parasitic capacitance of the inductor by adding more area between layers of rolling to get more capacitive area. This design does not increase the overall form factor for the inductor, as the parasitic capacitors are within the two vertical traces in Figure 4.9. With this design, the overall parasitic capacitors reach a maxim value of 320pF with the constrains of the dimension of the inductive pattern within 11cm long and 23mm wide.



Figure 4.9 Revised pattern version 1 for inductor

The characterization of the parasitic capacitance is verified with two methods. One is to connect the rolled inductor to a circuit in Figure 4.10. In the circuit, L1, R3, C1 form as the overall model of the inductor. V1 is a signal generator generating a step signal for a voltage from 0 to 5V. A transient response of the circuit is recorded with an oscilloscope measuring the voltage between the two ends of the inductor. A simulation of the circuit is done on a software LTspice. The parameters of the inductor, including C1, L1 and R3 are tuned for the simulation to match the

measured data, so that the parameters C1 and L1 represent the real parasitic capacitance and the inductance of the rolled inductor.

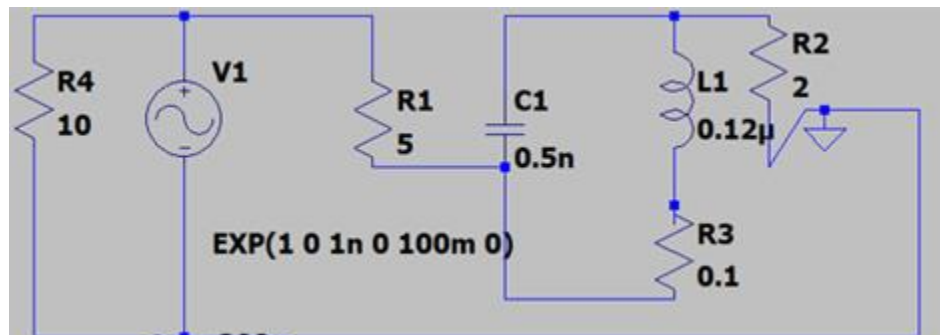


Figure 4.10 Testing circuit for rolled inductor

The measured data and the simulated data for the transient response for the rolled inductor is shown in Figure 4.11. The voltage response of the rolled inductor shows that the voltage spikes up in the beginning of the step when the signal is triggered from 0 to 5V. Then, at about 20ns, the voltage reaches the peak value, as about 2.4V or 2.5V. This type of responsive behavior is because the rolled inductor has an inductor-capacitor-resistor loop internally. The LCR response in terms of time has a damping effect in this circuit. The frequency of the response is called damped resonance frequency or the damped natural frequency. It is the frequency the circuit will naturally oscillate at if not driven by an external source. After the voltage reaches the peak value, it goes down into below zero and then comes back and resonant until it reaches a relatively stable value. Eventually the voltage of the rolled inductor is determined by the ratio of the inner resistance R3 and the resistance of the rest of the circuit where in this circuit it is the sum of R1 and R2.

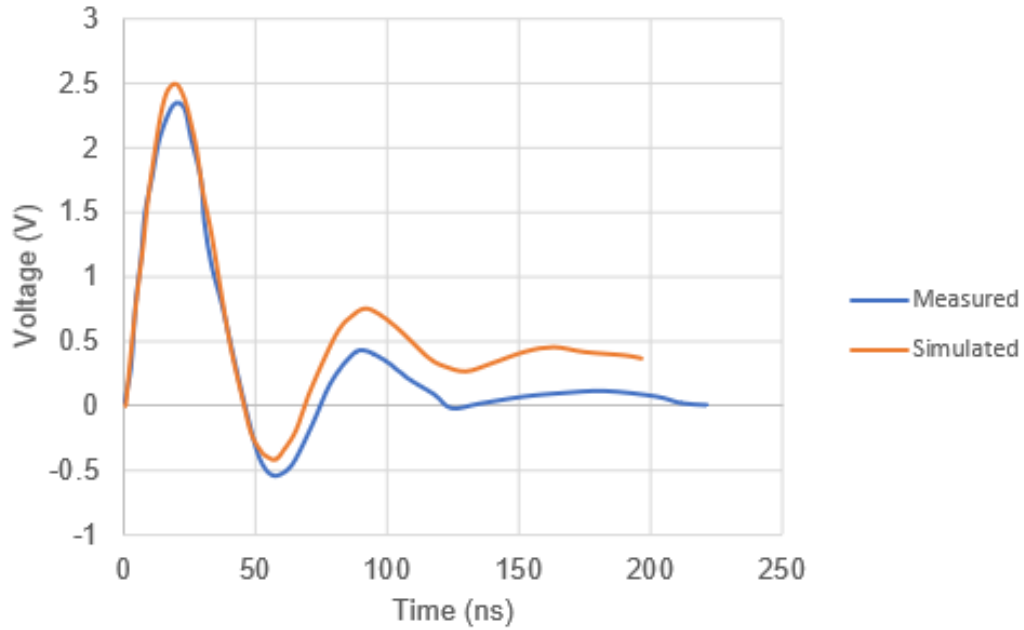


Figure 4.11 Transient response for measured and simulated data

Another method to measure the parasitic capacitance is to cut the top part of the metal trace, shown in Figure 4.12. In this way, the inductor is cut open while remaining the capacitor when the pattern is rolled. So the corresponding circuit of the rolled inductor, in this case, is only a capacitor with its resistance in parallel to it and the effect of the inductor is eliminated. The testing of the capacitance of the capacitor could be done by either calculating the capacitance from a RC circuit's time constant when signaled with a step signal and recorded the transient response of the capacitor in an oscilloscope, or via a LCR meter. The methodology of the testing is to be able to test one parameter in two different methods to agree with each other so the testing results are accurate.



Figure 4.12 Cut pattern to measure parasitic capacitance of the rolled inductor.

Another design for the large area of the parasitic capacitor comes from the additional area outside of the triangle of the pattern for the inductor, shown in Figure 4.13. The same mechanism applies to this type of the pattern as the ones with the additional pads inside of the triangle area. In this design, the overall area of the additional pads could be slightly larger depending on the detailed design of them and may result in more parasitic capacitance, with the limit of the boundaries to be within the dimension of the rolled width. The size of the pads could also affect the parasitic capacitance simply because of the effective size covered between layers of rolling forming the parasitic capacitance. According to the experiment, the parasitic capacitance could reach about 400pF at an overall dimension of the whole pattern of the inductor to be 12cm long and 23mm wide.



Figure 4.13 Revised pattern version 2 for the rolled inductor.

The above two types of the designs for the inductor could be combined, shown in Figure 4.14. This design shows a larger parasitic capacitance compared with the previous two designs, the ones with additional inner pads and outer pads. In the experiment, given the same overall dimension as of the previous two patterns, the parasitic capacitance of this design reaches 700pF but with a sacrifice of the inductance because the current is spread from the gold metal trace to the pads, resulting a wider effective width compared with the width of the gold trace. According to the experiment done above, the wider the metal trace is, the smaller the inductance is. The smaller inductance contributes to a smaller quality factor, so the overall detected signal goes smaller. The other effect of the smaller inductor is that the resonant frequency of the pH sensor goes up making the overall bandwidth of the working frequency moves higher. This problem gives more pressure to the design of the handheld device to meet the required specification of the bandwidth.



Figure 4.14 Revised pattern version 3 for the rolled inductor.

While the addition of the pads into the pattern of the inductor gives a better parasitic capacitance of the rolled inductor, making the bandwidth smaller, however, there is still an issue with the design, which is the relatively low quality factor because of the high resistance. Making the thickness of the metal film larger make the resistance decrease but with an increase of cost of fabrication. More improvement needs to be taken to address this issue with the resistance of the inductor.

The triangled pattern for the inductor, with or without the additional pads, consists of two coils, one left and one right, and the parasitic capacitor in between layers. The rolled inductor consists of two coils, shown in Figure 4.4, the left one L_1 and the right one L_2 . The total inductance is $L = L_1 + L_2 - 2M$, where M is the mutual inductance of the two coils. A typical rolled inductor shows a $L_1 = 0.43\mu H$, $L_2 = 0.36\mu H$ and $L = 0.5\mu H$. Note the geometry for this design is with a length of 14cm, a width of 23mm, a metal-trace length of 1mm. While the two coils relatively split the resistances contributing to the total resistance. With only one left side, the individual inductor has a higher quality factor than the two coils together. This gives a new method of design of the inductor for the pH sensor, even though the fabrication is more complex

than the original design, because if the inductor only has one side in the planar pattern, after it is rolled, the two ends of the metal trace would be at the inner and outer side of the rolled cylinder, making the connection to the electrodes difficult. This brings more challenge to the fabrication process.

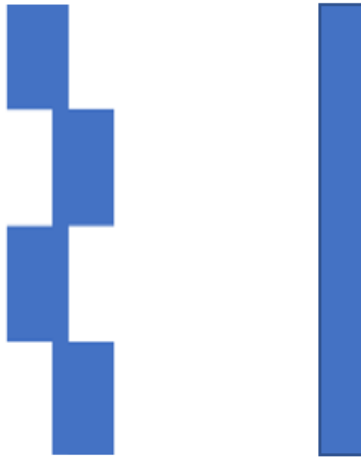


Figure 4.15 Two version of patterns for single-line inductors

Two versions of the patterns for single-line inductor are shown in Figure 4.15. The left one has four additional pads to increase the parasitic capacitance of the inductor, while the right one is rectangular. The experimental data are shown in Figure 4.16 to compare the inductance between rectangular patterned inductor and non-rectangular patterned inductor. With similar overall dimensions, the rectangular patterns show higher inductances. Further investigation shows the inductor made of rectangular pattern has a relatively large parasitic capacitance compared with the ones made of triangle patterns and no additional pads, even though still smaller than the ones made of rectangular pattern and with additional pads. The resistance of the single-line inductor is much smaller than the triangled version, giving the rolled inductor a high quality factor. The benefit of quality factor shows more significant in mid-range detection of the signal.

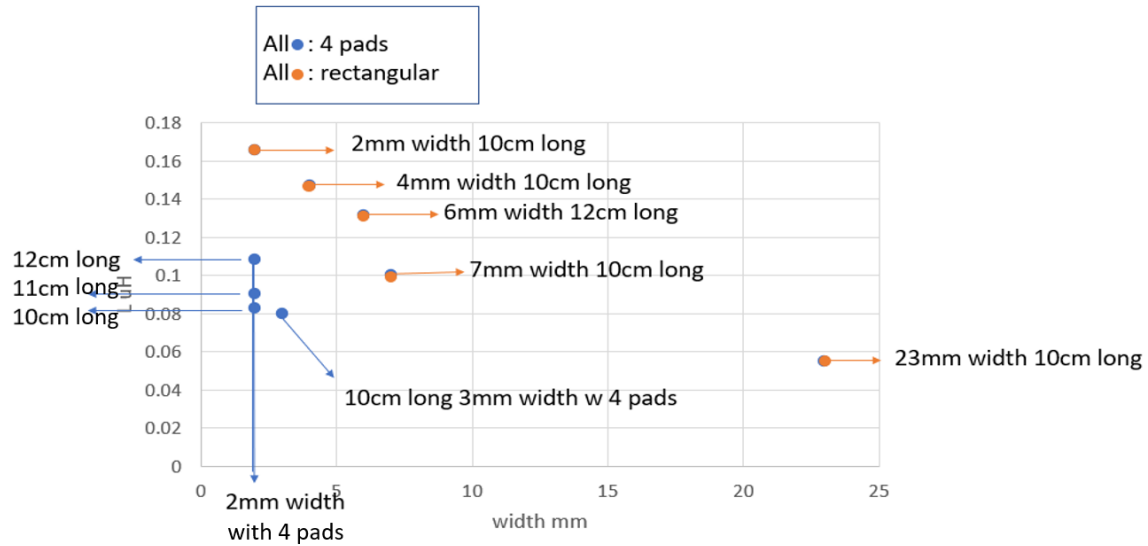


Figure 4.16 Comparison of inductance between rectangular patterned inductor and non-rectangular patterned inductor.

A new pattern is then designed to enhance the quality factor, shown in Figure 4.17, where the connections between the electrodes and the inductor are modified to accommodate the fabrication process. The far end of the inductor goes to the inner side of the rolled capsule while the far end of the electrodes is exposed to the outside surface of the capsule. To form a circuit, the two ends are connected by flipping the inner side and attaching to the outer side. Then, Eudragit solution is dropped on to seal them together. In this way, a LCR circuit is built and ready to be tested. Note that in this design, the right end has a longer edge than the left end's edge. It is to meet the accuracy requirement from the fabrication, especially in the process of rolling, where a mismatch of the dimension could happen making the two ends not able to be connected. The rolling process's dynamic change of the rolling force, or the defects of the film, could make the rolling turns to be over or less than the designed specs. The wide edge could cover about 150 degrees of angular mismatch, giving a better yield in the fabrication process.

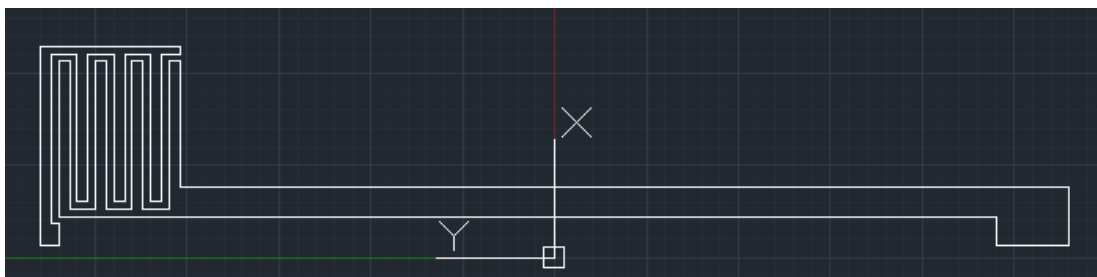


Figure 4.17 New pattern of the improved pH sensor

4.4. Fabrication of the pH sensor

3 g of gelatin was dissolved in 25 g of distilled water for 20 minutes at 70 °C. The solution was capped with aluminum foil to prevent the evaporation of water. 1.63 g of glycerol was added into the solution, followed by magnetic stirring (700 rpm) for 20 minutes at 70 °C. The solution was then poured onto the coating machine and spread evenly. A fan was used to blow the air 50cm above the solution for 6 hours to dry the film. 2.5g of Eudragit was dissolved into 17 g of absolute ethyl alcohol. The solution was capped with aluminum foil to prevent the evaporation of water. After 30 minutes the solution was placed under magnetic stirring (700 rpm). A fan was used to blow the air 50cm above the solution for 1 hour to dry the film. After the substrate had dried, coat the gelatin film on the apparatus with the Eudragit L100 solution made in step 2. Wait for 1 hour to dry with a fan blowing air 50cm above. After it dries, the substrate was peeled off and flipped over. The substrate was coated on the other side with Eudragit solution.

The substrates of pH sensor were then placed in a vacuum chamber of gold sputtering machine, where gold was deposited on the substrate through the shadow mask, with a thickness of 800 nm. Finally, the shadow mask was removed.

Prepare the gelatin coating solution by dissolving 2 g of gelatin in 15 g of distilled water. Coat the surface of the sample that contains the electrode patterns with 1mm thick gelatin coating solution by dropping and let it dry for 1 hour. Coat the surface of the substrate that contains the antenna patterns with Eudragit L100 solution using spraying coating technology and let it dry for

15 minutes. Note that the two ends of the pattern, one from the electrodes and the other one from the inductor's far end are not coated so they could be further stick together.

Roll the sample using a stainless-steel stick (4mm in diameter) to form a cylinder shape. The stick is inserted in a holder that has two walls at 2mm more than the film's width. The surface with gold pattern faced outside and the end with antenna should be rolled first. The film is taped on to the stick at one end and stretched at a force 0.59N. Use the Eudragit L100 solution as glue to make the end of the sample with electrodes stick to itself. Flip the far end of the inductor at the inner side and attach to the outer side to contact the far end of the electrodes. Then, Eudragit solution is dropped on to seal them together. Cut the tape and remove the sample from the stainless-steel stick.

4.5. Characterization of the pH sensor

The testing circuit to detect the signals from the pH sensor is developed. The previous bench used a signal generator, an amplifier, and an oscilloscope but the sweeping and recording process takes a significant amount of time as individual frequency and the corresponding signals are recorded manually, when the typical sweep takes up to 4000 data points for the frequency and the voltage. The new bench is improved by using a spectrum analyzer with a tracking generator integrated, where the tracking generator could sweep automatically, and the voltage/signal information could be recorded along with the corresponding frequencies in the spectrum analyzer. The schematic is shown in Figure 4.18. The spectrum analyzer sweeps and records the data automatically. When the tracking generator sweeps across the bandwidth, such bandwidth could be tuned along with the signal source power, sweeping time, delays between two frequencies. The data of frequency and signal strength in dBm are transferred to a computer for further analysis to find the resonant frequencies of the pH sensor. The signal strength is compared from the computer between tests with and without the pH sensor, and a spectrum of the difference between the two sets of signal values is plotted in terms of frequencies to find the local peak value, where it is the resonant frequency of the pH sensor. As mentioned previously, resonant frequency has a one-to-one relation to the acidic level of the solution being tested, so

the pH value of the environment could be tested when compared the resonant frequency measured and calculated from the data to the calibrated frequency-pH value relation.

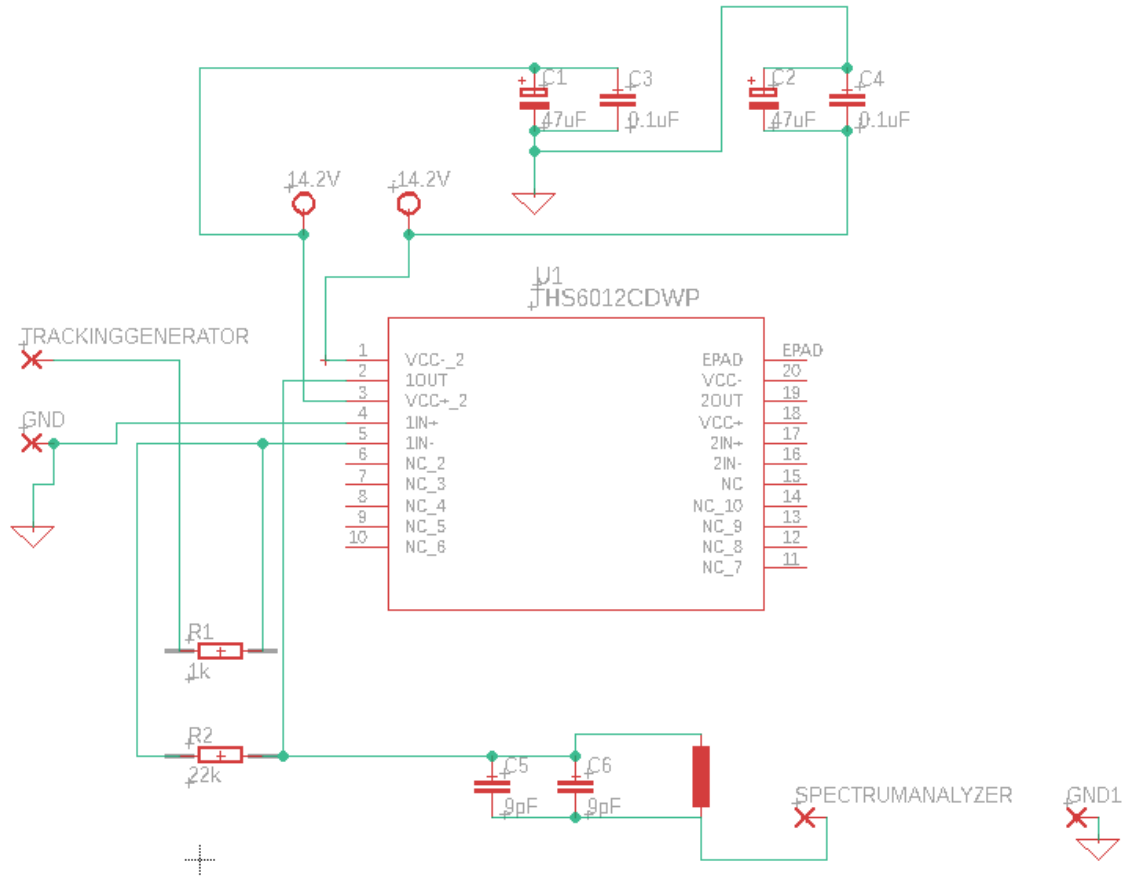


Figure 4.21 Schematic of testing bench for the reading circuit.

An amplifier JHS6012CDWP was used in the reading circuit to further differentiate the signal from noises. The output of the tracking generator goes through a resistor R1 and then connects to the negative input of the amplifier. The ground of the tracking generator goes to the positive input of the amplifier. The amplifier works with a power supply of 14.2V DC. The power source is filtered with four capacitors C1, C2, C3, C4 to get a relatively clean DC voltage. The output of the amplifier goes to the reading circuit, mostly a LC circuit, and the other end of the circuit goes to the input of the spectrum analyzer. The ground of the input of the spectrum analyzer is connected to the ground of the tracking generator. Figure 4.19 shows the difference between high-power input and low-power input. An artificial pH sensor is used to verify the signal

strength of the circuit. The artificial pH sensor consists of a standard capacitor connected to a rolled coil with the same geometry as the designed inductor for the pH sensor. Copper wire is used to replace gold metal trace for a better resistance, which results in a better quality factor of the coil so other parts of the testing setup is easy to develop with. For the amplified input as 0dBm, the sensor's signal strength reaches about 20dB, while in the low input power setup (without an amplifier), the signal strength is about 10dB. The additional amplifier significantly improves the quality of the signal strength, giving more robust range in terms of detecting distance. Note that in Figure 4.19, the artificial sensor was placed 2cm away from the reading antenna. As signal attenuates with longer distance between the sensor and the reading antenna, an amplifier could boost the signal and allow the bench to detect the artificial pH sensor at a longer distance.

The shape of the spectrum plotted in Figure 4.19 is important because it is relatively symmetric across the frequency bandwidth. Experimental study shows that the symmetric spectrum only occurs when the resonant frequency of the pH sensor and the resonant frequency of the reading circuit are the same. Otherwise, the plot is asymmetric, where this phenomenon helps to identify the resonant frequency of the edible pH sensor.

Also, the signal strength is the largest when the two resonant frequencies are the same. This phenomenon is also important because when the two resonant frequencies are the same, the detecting range could be larger than the conditions when the two frequencies are different. When the reader and the edible pH sensor are further away from each other, the signal attenuates fast, which would be further studied later in this chapter. So, an innovation for the circuit development is to change the resonant frequency of the reading circuit while sweeping. In the circuit shown in Figure 4.18, changing the capacitors C5 and C6 would change the resonant frequency of the LC circuit in the reader. By graduating changing the capacitance would change the resonant frequency of the reader correspondingly while sweeping frequencies to detect the signal for the pH sensor. The spectrum plots are captured and compared to find the maxim peak of each plot and the maxim peak among all the peak values from different plots happens when

the two resonant frequencies are the same. In this method, the signal strength could be boosted to its extreme for the maxim range of distance of detection. In the development of the reading circuit and the process of testing, different capacitors are used to achieve the function of getting different resonant frequencies of the reading circuit. Later in the study, varactors are used to tune the capacitance at an automatic and more detailed way. The capacitance could vary into thousands of values, making thousands of resonant frequencies for the reading circuit. This method of using varactors massively improves the resolution of the sweeps.

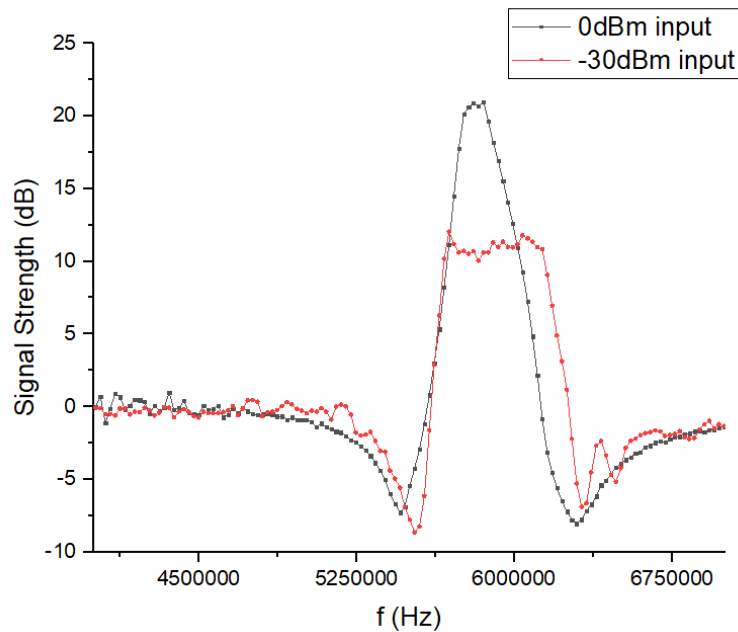





Figure 4.22 Signal comparison between high input power and low input power.

Beside adding the amplifier, optimization of designs in the reading antenna also improves the signal strength of the setup. Table 4.4 gives a few designs of inductors for the reading antenna, including a few planar inductors with different inner diameter, and a cylindric inductor with a similar size as the other two. According to the table, planar coils have higher inductances compared to cylindric coils, thus have higher quality factors given the same dimensional boundaries and resistances. So, further study of the reading inductor is focused on the planar coils, rather than the cylindric coils. Note that getting a high inductance and a smaller resistance

is not enough for the purpose of the reader, even though they contribute to a larger quality factor for the reading antenna, and a higher quality factor usually promises a narrow and sharp detecting bandwidth to get a better signal strength. Sensitivity of the reading antenna in terms of the distance between the reader and the edible pH sensor should be optimized to reach a relatively maxim signal strength across the working range of the tests, because the real working condition carries out at the near- and mid-range distance when used in the human body, where it is the distance between the edible pH sensor in the stomach and the reader out side of the human body.

Table 4.4 Examples of designs of reading antennas.

Inductance (uH)	30.6	32.5	11.3
			

The signal strength of the pH sensor detected from the reading antenna is defined as the powered transferred between the reading antenna to the pH sensor. The transferring power P_L is

$$P_L = \frac{\omega^2 M_{23}^2 V_s^2 R_L}{[\omega^2 M_{23}^2 + (R_2 + R_s)(R_3 + R_L)]^2},$$

where M_{23} is the mutual inductance between the two inductors, R_2 , R_3 , R_s , R_L are the resistances of the two coils, V_s is the input voltage and ω is the angular frequency of the circuit. While improving the resistance, the mutual inductance is the key parameter to improve the signal strength in terms of detecting range.

A simulation of mutual inductance in terms of planar coils' inner diameter was done in MATLAB to analyze the performance in a range of distance, from near field to middle field, shown in Figure 4.20. Inductors with smaller inner diameters have larger mutual inductance in the near field but suffer in the middle field, resulting in a high signal strength in the near field and low in middle field. Large inner diameter contributes to a lower mutual inductance for the planar inductor but maintains a steady decline of mutual inductance over the range of distance, making the inductor perform better in the middle field. Note that all inductors used in the simulation have the same number of turns (7 turns) with the same wire width and spacing.

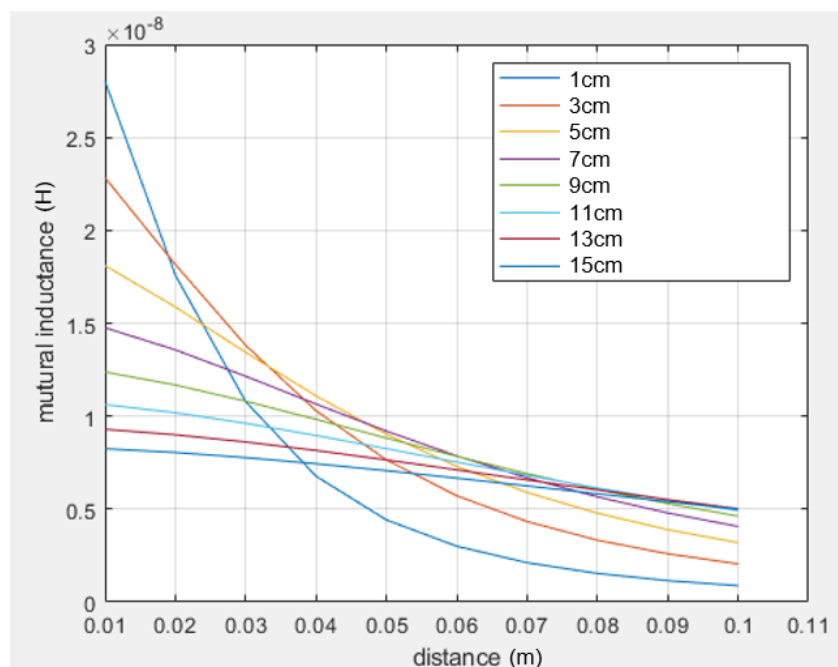


Figure 4.23 Simulated mutual inductance vs. distance relative to different inner diameter of the planar coil.

After the optimization of the testing circuit and the reading antenna, the artificial pH sensor was tested, and the results are in Figure 4.21. The resonant frequency of the artificial pH sensor is about 5.6 MHz. When the artificial pH sensor is at 2cm away from the reading antenna, the signal strength is about 27dB. The signal strength attenuates when the artificial pH sensor is moved away from the reading antenna. At 6cm, the artificial pH sensor is still detectable, with

about 2dB signals, which is large enough to differentiate from the environmental noise. Further study shows that at about 10cm distance, the signal is too small to differentiate from the background noise.

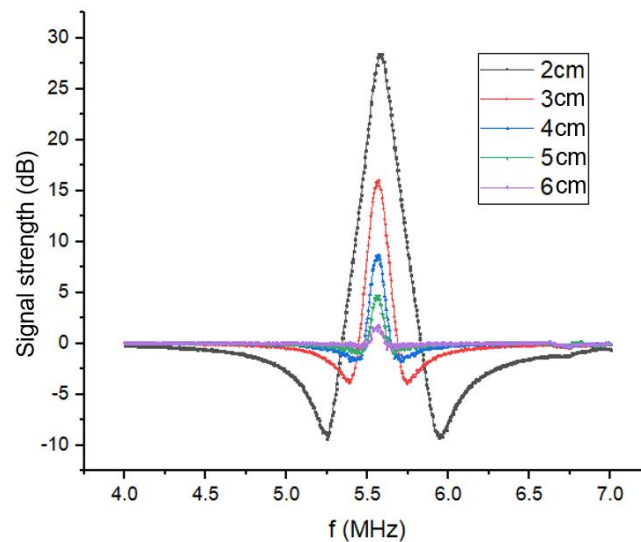


Figure 4.24 Signal strength of an artificial pH sensor vs. frequencies at different distances.

Further development of the testing bench was outsourced to a private company to achieve better performance in terms of detecting range, ease of usage, auto calibration and small form factor. A handheld device is developed from the private company to replace the existing testing bench with more merits, which would be shown in the later part of this chapter.

4.6. Result and Discussion

A new design of the pH sensor was demonstrated to accommodate the issue with form factor, making the whole device practical for patients to swallow like a capsule. The individual parameters of the pH sensor were designed and optimized to improve the overall performance of the sensor, fitting into a practical range of bandwidth, achieving maximum signal strength and detecting range.

After the verification with artificial pH sensor, a real pH sensor was tested with the testing bench. The pH sensor is placed at 2cm away from the reading antenna and the analyzed data are plotted in Figure 4.22. The resonant frequency of the pH sensor is about 4.18 MHz with a signal strength of about 0.52 dB. Note that the frequency spectrum of the pH sensor is symmetric relative to frequency. The issue with this bench is that the signal is small in a long distance between the reader and the pH sensor, due to the limited input power from the reading circuit that makes the signal not strong enough to different from noise in this range of distance. The improved testing setup, a handheld device is to solve this issue.

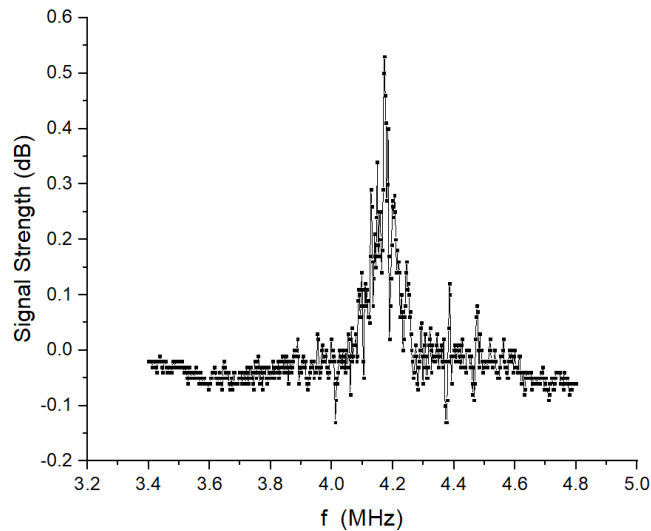


Figure 4.25 Signal strength of a real pH sensor vs. frequencies at 2cm distance.

The handheld device is used to test the resonant frequency of the pH sensor. The setup of the bench is shown in the Figure 4.23. A beaker is placed on top of a petri dish for elevation so that the handheld device's antenna could face the pH sensor in the beaker at its axial direction. Some acidic solution made from hydrochloric acid and water, finely tuned with ratios to get a certain pH value of the solution, is put into the beaker along with the pH sensor. The handheld device is placed in front of the pH sensor at a distance range from 2 cm to 10 cm, depending on the specific testing condition. The usage of the handheld device comes with pressing the button

on the device shown in Figure 4.23 and followed by booting the system. Then, double click the button after moving the whole handheld device to a vacant space without the edible pH sensor anywhere near to it. The action of double clicking triggers the calibration process of the handheld device. After it is calibrated, put the handheld device to the front the pH sensor at a distance. Then, press the button again to perform the test. The device would sweep and scan the bandwidth of interest and detect the signal transmitted back to the reader. The signal-frequency data are compared with the calibration data to plot the differential signal-frequency spectrum, also shown in Figure 4.23. A local maxim peak is found to be the estimated resonant frequency of the pH sensor.

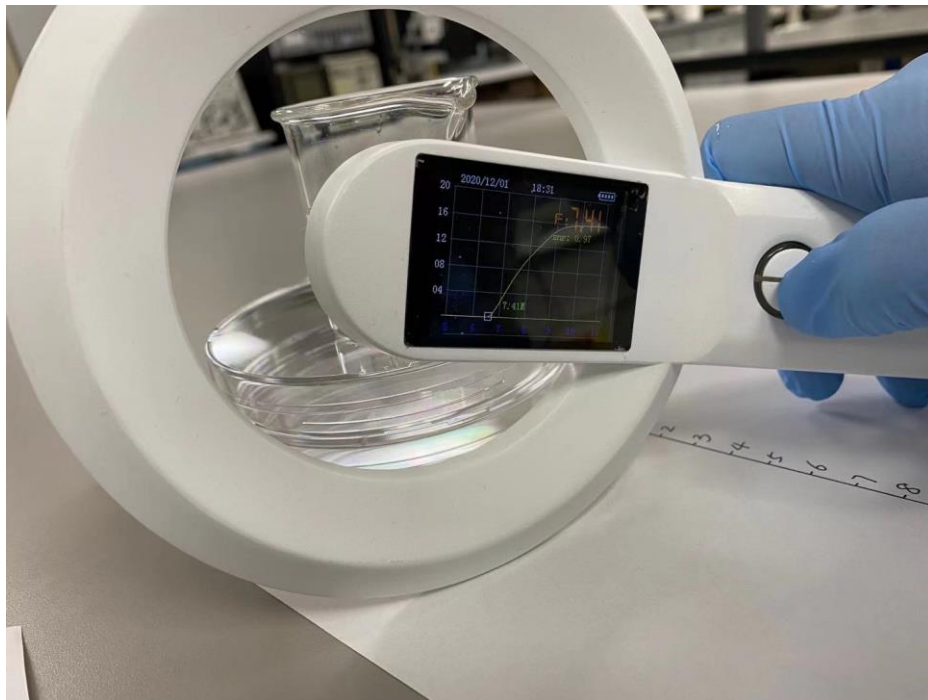


Figure 4.26 The setup for testing the pH sensor with a handheld device.

A typical example of the plot output from the handheld device after the test is shown in Figure 4.24. In the picture, there is a LCD screen showing the plot of signal strength and the sweeping frequencies. The ring surrounding the LCD screen is the supporting frame, in which there is the reading inductor. The solution of the hydrochloric acid has a pH value of 3. In the

background of the figure, the edible pH sensor is dipped into the beaker filled with hydrochloric acid solutions. The signal strength's unit is 0.75mV which is the resolution of the handheld device and the frequency has a certain bandwidth. A local dip is found in the plot and the peak point is marked with a frequency of 8.05MHz.

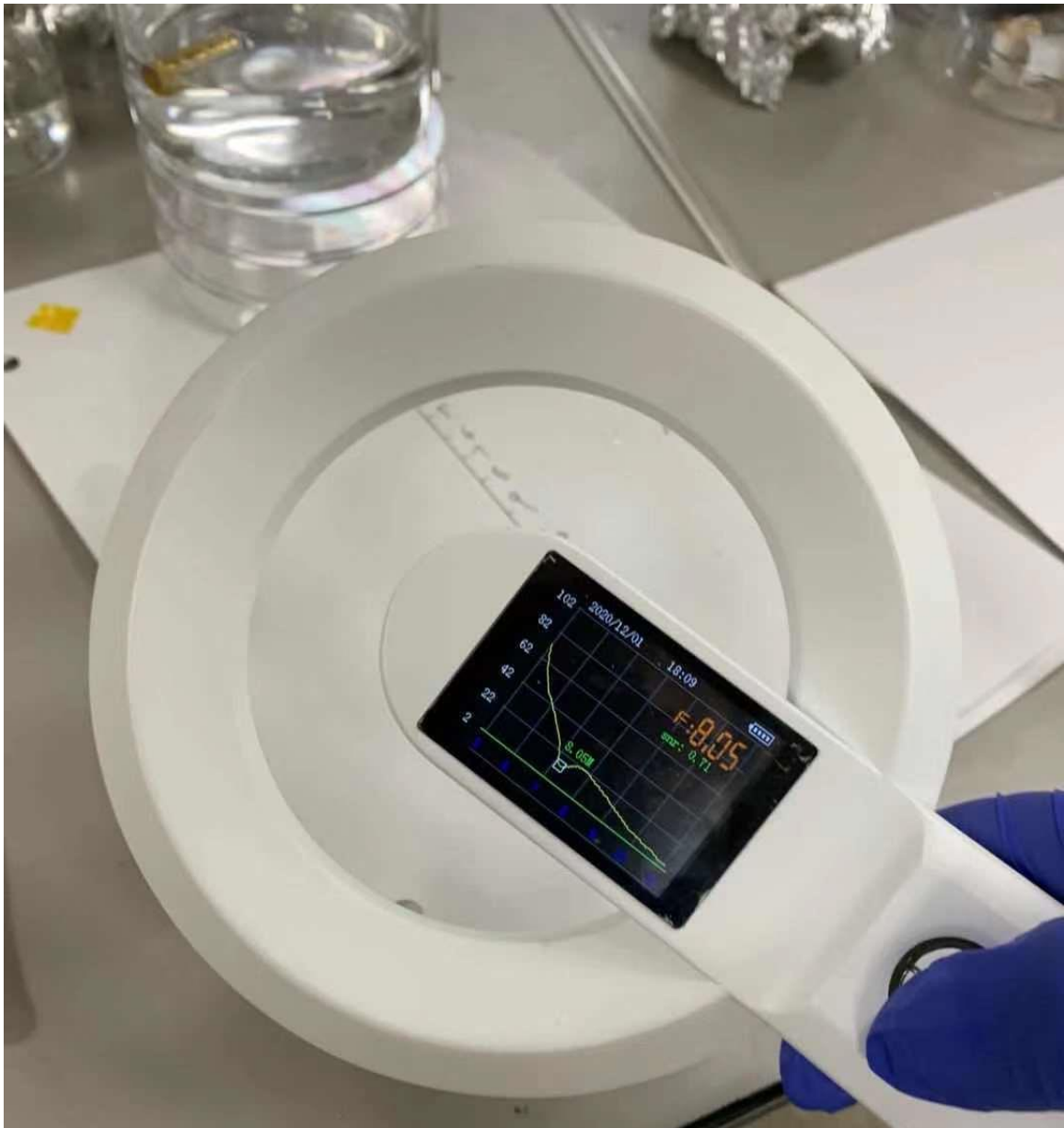


Figure 4.27 The testing result from the handheld device after testing a pH sensor in a solution of hydrochloric acid with a pH value 3.

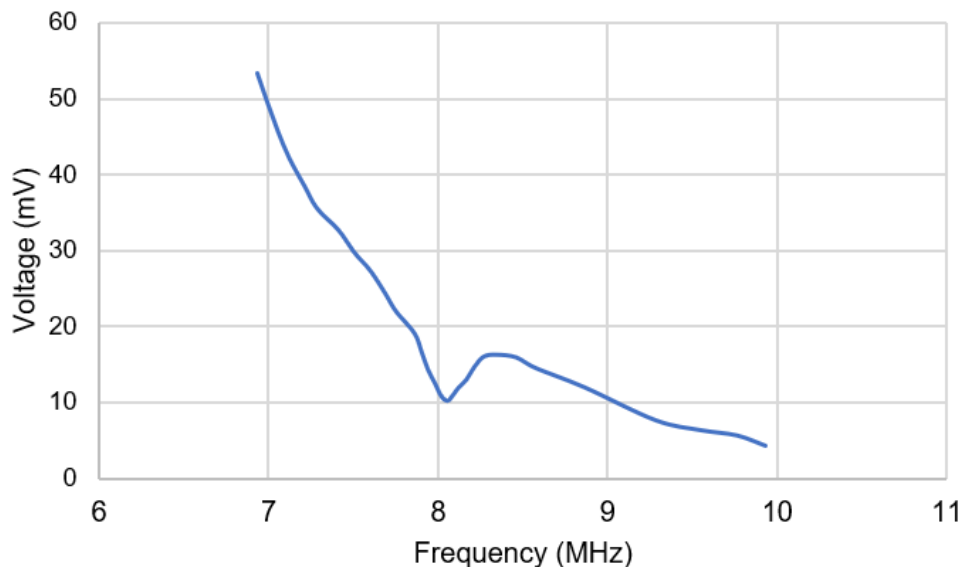


Figure 4.28 Voltage-frequency response of the pH sensor in a solution of hydrochloric acid with a pH value 3 recorded from the handheld device.

The corresponding plot shown in Figure 4.24 is output from the handheld device to replot in Figure 4.25, for more clarification. The unit in the vertical axis is converted to voltage in mV. Across the sweeping bandwidth, the voltage range of the signal is about 50mV and the local valley happens at about 8MHz. At this frequency, the local peak value of the voltage is about 10mV. Different peak or valley frequencies represent different resonant frequencies of the pH sensor, and further representing the different pH values. A repeated series of testing in solutions with different pH values is carried out.

5 SUMMARY AND FUTURE WORK

5.1. Summary

A new class of electronic materials from food and foodstuff was developed to form a “toolkit” for edible electronics along with inorganic materials. Electrical components like resistors, capacitors and inductors were fabricated with such materials and tested. The material sciences of food industry, design and fabrication of electronics and biomedical engineering was discussed by

demonstrating edible electronic materials, components and devices such as filters, microphones and pH sensors. Applicable devices such as filters, microphones and pH sensors were built with edible materials. Among the applications, a wireless edible pH sensor was optimized in terms of form factor, fabrication process and cost. The design of individual components of the edible pH sensor is studied to achieve the balance between performance and cost. In the development process, the testing circuits are built and optimized for the characterization of individual components and for the pH sensor. A few versions of pH sensor are developed to counter the difficulties in bandwidth, signal strength, quality factor et al. A few iterations of reading circuits are developed to accommodate the real-life usage of the testing device.

This study of edible food-based material and its applications in the medical electronics opens a door for a new platform for making low-cost, bio-compatible and bio-dissolvable electronics. Because of the unique electrical and mechanical properties, the design and fabrication of electronic devices made from these types of materials are different from traditional semiconductor industrial standards.

5.2. Future Work

The testing of the new handheld device is still ongoing and would be in the future work, to successfully detect the pH sensor at a middle range (about 10cm). Scenarios of different orientations between the reader and the edible pH sensors should be studied in terms of detecting range. The sensitivity of the edible pH sensor and the reading circuit should be considered in the future study. The handheld device for pH sensor needs to be optimized to work with different real-life situations including animal experiments, human body experiments and clinical trials. The eventual goal for this study is to develop a usable system consisting of an edible pH sensor and the related handheld reading device to meet the market need of testing patients' pH values in the GI tract as it goes.

The pH sensor's form factor could be potentially even smaller. Basically, it is a LRC circuit, and the inductance is at micron henry level, the resistance is within 1 ohm, and the

capacitance is at nano farad level. If we can make a LCR circuit within this range in a silicon wafer, in compliance with massive production procedures of the traditional semiconductor industry, the fabrication of the pH sensor could potentially follow “Moore Law” where every year or eighteen months, the density of the device doubles, meaning that the cost of individual pH sensor could be reduced to half, while still supporting the same performance. Eventually, the pH sensor could be shrinking to a small size as in 1mm of overall dimension, making the cost of fabrication decrease significantly. Another benefit of having a smaller form factor of the pH sensor is to be able to integrate onto commercial capsules. Doing so could be more convenient to patients as they do not need to take the pH sensor separately from other medical pills or capsules. While regular pills could have different functional materials to treat disease, the pH sensor glued on to the surface of the capsule could measure the pH value of the stomach when the patient takes pills. It could also monitor the patients’ pH values after the take regular medicine. Some patients do not feel comfortable pills and refuse to. So, monitoring the pH value after they swallow could validate that they have taken the pills, which could help the doctors track the intakes of the medicine.

The application of the edible electronic capsules could go further beyond the monitoring of the pH values. If the sensing electrodes could sense temperature, acceleration, or any other parameters that are useful in diagnosis in the GI tract, more and more functions integrated into the edible electronic capsules could be engineered.

REFERENCES

1. A. Wang, S. Banerjee, B. A. Barth, Y. M. Bhat, S. Chauhan, K. T. Gottlieb, V. Konda, J. T. Maple, F. Murad, P. R. Pfau, D. K. Pleskow, U. D. Siddiqui, J. L. Tokar, S. A. Rodriguez, and Asge Technology Comm, 2013. Wireless capsule endoscopy. *Gastrointestinal Endoscopy* **78** (6), 805-815.
2. Richard J Saad, 2016. The wireless motility capsule: a one-stop shop for the evaluation of GI motility disorders. *Current gastroenterology reports* **18** (3), 14.
3. P Gonzalez Carro, J Picazo Yuste, S Fernandez Diez, F Pérez Roldán, and O Roncero Garcíá-Escribano, 2005. Intestinal perforation due to retained wireless capsule endoscope. *Endoscopy* **37** (07), 684-684.
4. Avraham Yitzhak, Michael Bayme, Zvi H Perry, and Solly Mizrahi, 2012. Small bowel perforation after capsule endoscopy in a patient with occult gastrointestinal bleeding and undiagnosed Crohn's disease. *The American surgeon* **78** (3), E159.
5. P.A. Minnesota Gastroenterology, SmartPill GI Monitoring System Price Quote, Available at <https://www.mngastro.com/sites/default/files/Price%20Quote%20SmartPill-15.pdf>, (2015).
6. Michael F Vaezi, Yu-Xiao Yang, and Colin W Howden, 2017. Complications of proton pump inhibitor therapy. *Gastroenterology* **153** (1), 35-48.
7. Steven O Ikenberry, Terry L Jue, Michelle A Anderson, Vasundhara Appalaneni, Subhas Banerjee, Tamir Ben-Menachem, G Anton Decker, Robert D Fanelli, Laurel R Fisher, and Norio Fukami, 2011. Management of ingested foreign bodies and food impactions. *Gastrointestinal endoscopy* **73** (6), 1085-1091.
8. Mitchell L. Schubert, 2014. Gastric secretion. *Current Opinion in Gastroenterology* **30** (6), 578-582.
9. D. Y. Khang, H. Q. Jiang, Y. Huang, and J. A. Rogers, 2006. A stretchable form of single-crystal silicon for high-performance electronics on rubber substrates. *Science* **311** (5758), 208-212.
10. R. Tang, H. Huang, H. Tu, H. Liang, M. Liang, Z. Song, Y. Xu, H. Jiang, and H. Yu, 2014. Origami-enabled Deformable Silicon Solar Cells. *Appl. Phys. Lett.* **104**, 083501.
11. Z. Song, T. Ma, R. Tang, Q. Cheng, X. Wang, D. Krishnaraju, R. Panat, C. K. Chan, H. Yu, and H. Jiang, 2014. Origami Lithium-ion Batteries. *Nature Communications* **5**:3140, DOI: 10.1038/ncomms4140.
12. Z. Song, X. Wang, C. Lv, Y. An, M. Liang, T. Ma, D. He, Y. -J. Zheng, S. -Q. Huang, H. Yu, and H. Jiang, 2015. Kirigami-based stretchable lithium-ion batteries. *Scientific Reports*, DOI: 10.1038/srep10988.
13. Xu Wang, Wenwen Xu, Prithwish Chatterjee, Cheng Lv, John Popovich, Zeming Song, Lenore Dai, M. Yashar S. Kalani, Shelley E. Haydel, and Hanqing Jiang, 2016. Food-Materials-Based Edible Supercapacitors. *Advanced Materials Technologies*.

14. W. W. Xu, H. K. Yang, W. Zeng, T. Houghton, X. Wang, R. Murthy, H. Kim, Y. R. Lin, M. Mignolet, H. G. Duan, H. B. Yu, M. Slepian, and H. Q. Jiang, 2017. Food-Based Edible and Nutritive Electronics. *Advanced Materials Technologies* **2** (11).
15. EFSA Panel on Food Additives and Nutrient Sources added to Food, 2016. Scientific Opinion on the re-evaluation of gold (E 175) as a food additive. *EFSA Journal* **14** (1), 4362.
16. Z. Li, R. S. Yang, M. Yu, F. Bai, C. Li, and Z. L. Wang, 2008. Cellular Level Biocompatibility and Biosafety of ZnO Nanowires. *Journal of Physical Chemistry C* **112** (51), 20114-20117.
17. Safaa Al-Hilli and Magnus Willander, 2009. The pH Response and Sensing Mechanism of n-Type ZnO/Electrolyte Interfaces. *Sensors* **9** (9), 7445.
18. Erdman Jr. J. W., I. A. MacDonald, and S. H. Zeisel, *Present Knowledge in Nutrition*. (John Wiley & Sons, 2012).
19. Ranulfo Lemus and Carmen F. Venezia, 2015. An update to the toxicological profile for water-soluble and sparingly soluble tungsten substances. *Critical Reviews in Toxicology* **45** (5), 388-411.
20. F. M. Vanin, P. J. A. Sobral, F. C. Menegalli, R. A. Carvalho, and Amqb Habitante, 2005. Effects of plasticizers and their concentrations on thermal and functional properties of gelatin-based films. *Food Hydrocolloids* **19** (5), 899-907.
21. J. Gao, J. D. Xu, L. E. Locascio, and C. S. Lee, 2001. Integrated microfluidic system enabling protein digestion, peptide separation, and protein identification. *Analytical Chemistry* **73** (11), 2648-2655.
22. K. Y. Lee, J. Shim, and H. G. Lee, 2004. Mechanical properties of gellan and gelatin composite films. *Carbohydrate Polymers* **56** (2), 251-254.
23. R. C. Rossi, C. L. Dias, E. M. Donato, L. A. Martins, A. M. Bergold, and P. E. Froehlich, 2007. Development and validation of dissolution test for ritonavir soft gelatin capsules based on in vivo data. *International Journal of Pharmaceutics* **338** (1-2), 119-124.
24. Maytal Foux and Meital Zilberman, 2015. Drug delivery from gelatin-based systems. *Expert Opinion on Drug Delivery* **12** (9), 1547-1563.
25. Melina Dick, Tania Maria Haas Costa, Ahmed Gomaa, Muriel Subirade, Alessandro de Oliveira Rios, and Simone Hickmann Flôres, 2015. Edible film production from chia seed mucilage: Effect of glycerol concentration on its physicochemical and mechanical properties. *Carbohydrate Polymers* **130**, 198-205.
26. <https://www.emf-portal.org/en/cms/page/effects-radio-frequency>.
27. H. Wu, M. Khmour, P. Apsangi, and H. Yu, 2017. High-Frequency Magnetic Thin-Film Inductor Integrated on Flexible Organic Substrates. *IEEE Transactions on Magnetics* **53** (11), 1-7.
28. D. O. Faigel, B. R. Stotland, M. L. Kochman, T. Hoops, T. Judge, J. Kroser, J. Lewis, W. B. Long, D. C. Metz, C. O'Brien, D. Smith, and G. G. Ginsberg, 1997. Device choice and experience level in endoscopic foreign object retrieval: An *in vivo* study. *Gastrointestinal Endoscopy* **43** (4), 334.

29. Douglas O. Faigel, Douglas F. Lake, Tracy L. Landreth, Catherine C. Kelman, and Ronald J. Marler, 2016. EUS-guided portal injection chemotherapy for treatment of hepatic metastases: feasibility in the acute porcine model. *Gastrointestinal Endoscopy* **83** (2), 444-446.
30. Samuel A Giday, John O Clarke, Jonathan M Buscaglia, Eun J Shin, Chung-Wang Ko, Priscilla Magno, and Sergey V Kantsevov, 2008. EUS-guided portal vein catheterization: a promising novel approach for portal angiography and portal vein pressure measurements. *Gastrointestinal endoscopy* **67** (2), 338-342.
31. Douglas O Faigel, Brian R Stotland, Michael L Kochman, Timothy Hoops, Thomas Judge, Joyann Kroser, James Lewis, William B Long, David C Metz, and Christopher O'Brien, 1997. Device choice and experience level in endoscopic foreign object retrieval: an in vivo study. *Gastrointestinal endoscopy* **45** (6), 490-492.
32. Constantin Cope, Douglas O Faigel, Gregory G Ginsberg, Hans A Timmermans, and Barry T Uchida, 2008. Creation of a gastroenteric anastomosis with endoscopy and percutaneous gastrostomy in pigs. *Journal of Vascular and Interventional Radiology* **19** (1), 124-128.
33. Rogier P Voermans, Brett Sheppard, Mark I van Berge Henegouwen, Paul Fockens, and Douglas O Faigel, 2009. Comparison of transgastric NOTES and laparoscopic peritoneoscopy for detection of peritoneal metastases. *Annals of surgery* **250** (2), 255-259.
34. Rogier P Voermans, Douglas O Faigel, MI van Berge Henegouwen, Brett Sheppard, and Paul Fockens, 2010. Comparison of transcolonic NOTES and laparoscopic peritoneoscopy for the detection of peritoneal metastases. *Endoscopy* **42** (11), 904-909.
35. Austin T Mudd and Ryan N Dilger, 2017. Early-Life nutrition and neurodevelopment: Use of the piglet as a translational model. *Advances in Nutrition* **8** (1), 92-104.
36. Given Imaging, SmartPill GI Monitoring System User Manual, Available at <https://fccid.io/O8PSMARTPILL/User-Manual/User-manual-2290351>, (2013).